LOYOLA UNIVERSITY CHICAGO 1870 AD · MAJOREM · DEI · GLORIAM
eCOMMONS

Loyola University Chicago
Loyola eCommons

Master's Theses | Theses and Dissertations

2017

Functional Studies of Novel Mosquito Stage-Specific Genes in the Malaria Parasite, Plasmodium Berghei.

Kaitlyn Kiernan
Loyola University Chicago

Follow this and additional works at: https://ecommons.luc.edu/luc_theses

 Part of the Cellular and Molecular Physiology Commons

Recommended Citation

Kiernan, Kaitlyn, "Functional Studies of Novel Mosquito Stage-Specific Genes in the Malaria Parasite, Plasmodium Berghei." (2017). *Master's Theses*. 3684.
https://ecommons.luc.edu/luc_theses/3684

This Thesis is brought to you for free and open access by the Theses and Dissertations at Loyola eCommons. It has been accepted for inclusion in Master's Theses by an authorized administrator of Loyola eCommons. For more information, please contact ecommons@luc.edu.

This work is licensed under a Creative Commons Attribution-Noncommercial-No Derivative Works 3.0 License.
Copyright © 2017 Kaitlyn Kiernan

LOYOLA UNIVERSITY CHICAGO

FUNCTIONAL STUDIES OF NOVEL MOSQUITO STAGE-SPECIFIC GENES IN THE MALARIA PARASITE *PLASMODIUM BERGHEI*

A THESIS SUBMITTED TO

THE FACULTY OF THE GRADUATE SCHOOL

IN CANDIDACY FOR THE DEGREE OF

MASTER OF SCIENCE

PROGRAM IN BIOLOGY

BY

KAITLYN KIERNAN

CHICAGO, IL

DECEMBER 2017

Copyright by Kaitlyn Kiernan, 2017
All rights reserved.

ACKNOWLEDGEMENTS

I would like to thank all the wonderful people who made this thesis possible. My mentor, Dr. Stefan Kanzok, provided the foundation and the encouragement I needed to accomplish all of my goals. He always pushed me to become a better student, researcher, and ultimately teacher. He taught me that with patience, persistence, and a lot of coffee, experiments eventually work out. I sincerely needed those pictures of his dog, Dora, to get through the long 14-hour days. I'd like to thank my committee members, Dr. Catherine Putonti and Dr. Jennifer Mierisch, for their constant support in and out of the lab. They were there for me when I was unsure and needed guidance to successfully navigate the program or when I needed antibodies (and I needed a lot of antibodies).

I'd also like to thank my fellow graduate students. Knowing that we were all in it together made the exhaustion so much more bearable. To all the lab members I had the pleasure of working with, thank you for keeping me sane and tolerating all of the pictures of my cat on a daily basis. I'd also like to thank all of my friends and family. I am so grateful that my dad raised me on good music; I would have never been able to pipet for hours on end without it.

Last but not least, thank you to the real MVP: my other half, Sean. As my level of craziness was inversely proportional to the time I had left in this program, he supported me through and through. I am so thankful to have him in my life. Thank you so much to everyone who supported me throughout my time here at Loyola.

To all of the past, present, and future scientists
for inspiring me to be who I am today.

TABLE OF CONTENTS

LIST OF TABLES

LIST OF FIGURES

CHAPTER I

INTRODUCTION

Malaria as a Global Threat

Malaria continues to be a serious threat to human health around the world. Taken from the World Health Organization's (WHO) recent World Malaria Report, there were an estimated 212 million cases and 429,000 deaths in 2015. Even with the $2.9 billion dollars pumped into the fight against malaria, there are still 91 countries and territories where the disease is considered to be endemic. Around 90% of the cases worldwide occurred in the WHO African Region with the remaining cases occurring in the WHO South-East Asia and Eastern Mediterranean Region. The WHO also found that only 30% of the population who is most at risk, children under the age of 5, received an antimalarial drug when testing positive for malaria infection.

The Malaria Parasite, *Plasmodium*

Malaria is a vector-borne disease that is caused by a protozoan, Apicomplexan parasite of the genus *Plasmodium*. There are five known species of *Plasmodium* that can infect humans: *P. falciparum, P. vivax, P. ovale, P. malariae* and *P. knowlesi.* Of these five species, *P. falciparum* is the most prevalent species in Africa, causing the most severe form of the disease, and consequently producing the highest mortality rates (Miller et al., 2002). *P. vivax* can also cause symptoms such as anemia; however, *P. vivax* is less virulent and not as widespread in the African region. Most of the *Plasmodium* species are transmitted by the bite of an infected female *Anopheles* mosquito (Oaks et al., 1991).

When an infected female mosquito takes a blood meal on a person, she injects invasive sporozoites from her salivary glands. The sporozoites travel through the bloodstream to the liver where they invade hepatocytes. Within the liver cells and over the course of 5-15 days, the sporozoites undergo schizogony and develop into tens of thousands of merozoites. The liver stage schizonts burst and release the merozoites into the bloodstream where they can then infect erythrocytes and continue reproducing asexually. Inside the erythrocyte, the merozoite continues to develop within a parasitophorous vacuole membrane (PVM) that consists of the membrane bilayer of the RBC. Over the course of 24-48 hours, the merozoite develops into a trophozoite and again undergoes schizogony. The schizont bursts and releases 10-20 merozoites into the blood where they infect new erythrocytes, continuing a cycle that causes the destruction of more RBCs and ultimately results in the symptoms that are characteristic of malaria (Miller et al., 2002) (Figure 1 RIGHT).

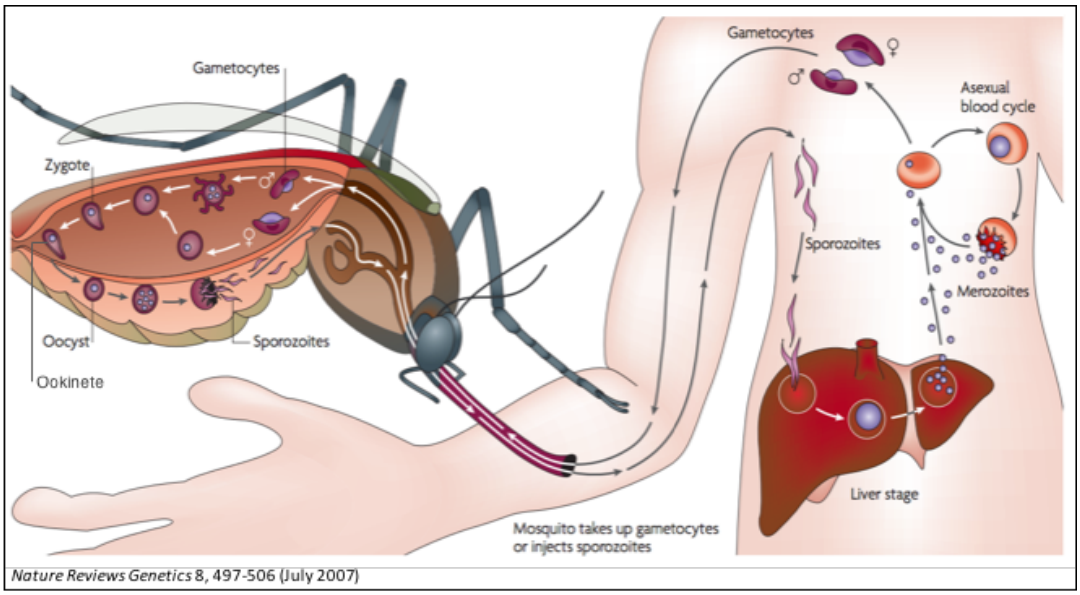

Figure 1 *Plasmodium* Life Cycle. (RIGHT) Asexual replication begins as an infected mosquito injects sporozoites into the mammalian host. The parasites replicate in the liver and the blood of the host. (LEFT) Sexual replication occurs in the mosquito as gametocytes are taken up from the blood of an infected host. The gametocytes undergo fertilization and develop into a zygote. The zygote develops into an ookinete which traverses the mosquito midgut lining where it develops into an oocyst. The oocyst produces thousands of sporozoites which travel to the salivary glands. (Su 2007).

A small subset of the parasite population will exit the asexual blood cycle and commit to sexual development. Instead of undergoing schizogony, the merozoites will develop into distinct male and female gametocytes. When a mosquito takes up these gametocytes with a blood meal, the gametocytes complete sexual reproduction within 15 minutes of entering the mosquito midgut. The female gametocyte egresses from the RBC and forms a macrogamete while the male gametocyte undergoes three rounds of DNA replication and releases eight exflagellating microgametes. The microgametes fertilize the macrogametes to generate a diploid zygote (Figure 1 LEFT).

Still part of the mosquito blood meal, the zygote develops into a motile form, called an "ookinete," over the course of the next 18-24 hours (Figure 1 LEFT). The parasite elongates into a polar, banana shape that enables the ookinete to pass through the blood meal and invade the epithelial lining of the midgut. The ookinete settles under the basal lamina of the midgut epithelial wall and undergoes multiple rounds of DNA replication and mitosis. Following a large scale cytokinesis event, the resulting oocyst contains thousands of haploid sporozoites. After 8-15 days, the oocyst bursts and releases motile sporozoites that travel to the mosquito salivary glands. Within the salivary glands, the sporozoites are primed for transmission and will be injected in to the next host during the mosquito's next blood meal (Oaks et al. 1991).

As drug-resistant parasite strains and insecticide-resistant mosquitoes are becoming more prevalent (Tun et al. 2015; WHO, 2010), research has been shifting towards the design of novel transmission blocking strategies. However, the only current transmission blocking vaccine candidate shows very little potential for long term protection and only targets one stage of the complex malaria parasite's life cycle (Gosling & Seidlein, 2016). As most of the research done on malaria focuses on development within the human host, very little is known about parasite

cell biology during mosquito stage development. In an effort to better understand and target *Plasmodium* transmission, our lab is currently studying the adaptive mechanisms underlying parasite survival and development, specifically in the mosquito vector.

The Model Rodent Malaria Parasite, *Plasmodium berghei*

The murine malaria parasite, *Plasmodium berghei,* has been established in the research community as an excellent model system for studying the mosquito stages of *Plasmodium* (Sinden, 1978). The *P. berghei* life cycle and morphological characteristics are comparable to those of the human parasite, *Plasmodium falciparum* (Sinden, 1978). The genome organization and metabolic pathways are also largely conserved between the rodent malaria parasites and the human malaria parasites (Janse *et al.*, 1994; Janse and Waters, 1995). On top of sharing many genetic and physical features, *P. berghei* can easily be used to study *Plasmodium* within the mosquito vector. As *P. berghei* is not infectious to humans, mosquitoes can be safely infected and studied in the laboratory. Working with mice is also much simpler and carries less ethical implications than working with humans.

Survival in the Mosquito Midgut

Upon arrival in the mosquito midgut and egress from the protective membrane of the RBC, *Plasmodium* becomes vulnerable in the inhospitable environment of the bloodmeal. Here, the parasite is exposed to an increased pH, a decreased temperature, the mosquito's own mounted immune response, digestive enzymes (Alavi *et al.,* 2003), reactive oxygen species (ROS), reactive nitrogen species (RNS), and a diverse microbial flora (Müller, 2004; Fang, 2004). As a result of these stressors, the mosquito acts as a bottleneck for *Plasmodium* where only very few parasites survive (Smith et al. 2014; Wang and Jacobs-Lorena 2013).

Defense Systems

Within the mosquito midgut, *Plasmodium* must defend itself from the harsh conditions, including cytotoxic ROS. Using one of the main antioxidant systems, the thioredoxin system, the parasite generates an environment in which it can cope with the oxidative stressors (Kanzok et al., 2000).

Thioredoxins and thioredoxin-like proteins comprise a large superfamily of proteins. Some of the proteins are ubiquitous redox proteins that play essential roles in many biological processes, such as the detoxification of reactive oxygen and nitrogen species and the redox regulation of protein function and signaling (Arner and Holmgren, 2000). Thioredoxins exchange electrons via the reduction/oxidation of dithiol/disulfide bonds, which maintains their cellular targets in a reduced state (Arner and Holmgren, 2000).

Within the thioredoxin superfamily, only a few proteins, such as Thioredoxin-1, have been well characterized (Nakao, 2015). Our lab has been studying the thioredoxin system of *Plasmodium* and searching for novel thioredoxin-like proteins that could play a role during parasite development in the mosquito.

Escape from the Midgut

Plasmodium must escape the midgut to avoid digestion with the rest of the bloodmeal. The parasite accomplishes this by developing into a polar, motile ookinete (Figure 2). This 18-hour transformation enables *Plasmodium* to traverse the epithelial cell lining of the midgut and move out of the harsh environment (Oaks et al., 1991). Without the ability to move and invade the epithelial cells, the parasites would fail to establish infection of the mosquito and would be digested with the rest of the bloodmeal.

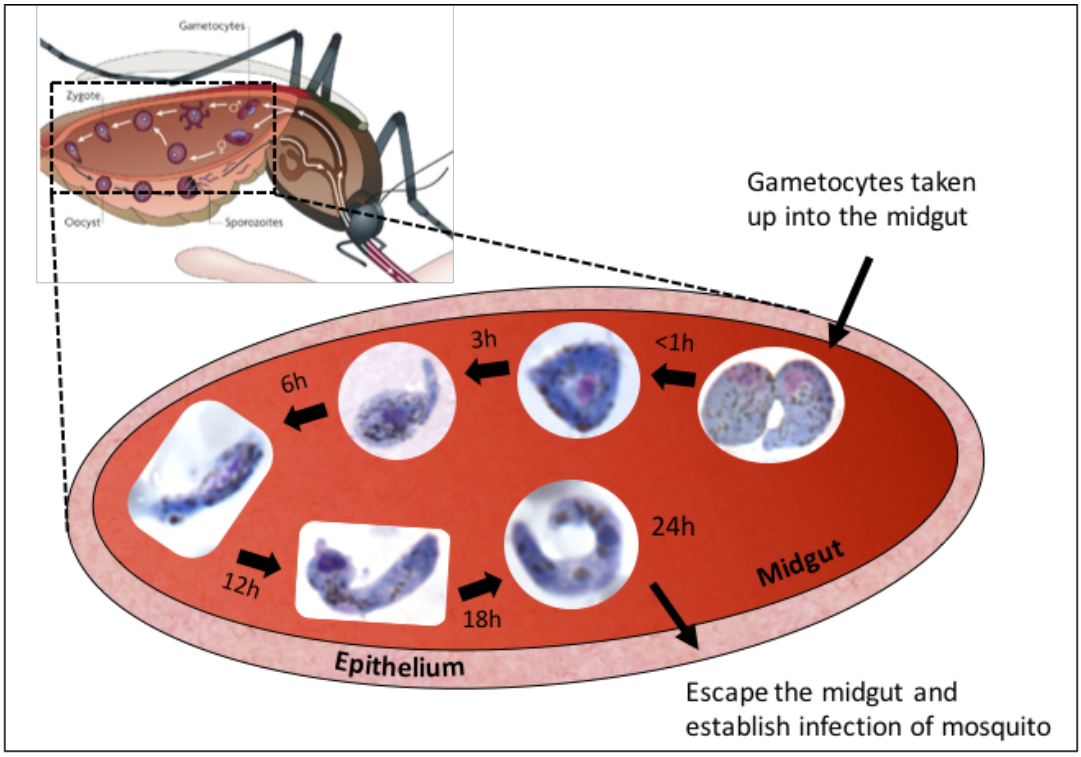

Figure 2 Ookinete Development in the Mosquito Midgut. Within 15 minutes of the gametocytes arriving in the mosquito midgut, they egress from their RBCs and undergo fertilization. Over the next 18-24 hours, the resulting zygote develops in a motile ookinete which can move through the bloodmeal and invade the epithelial lining.

A complex network of cytoskeletal organelles and filaments located underneath the plasma membrane, called the inner membrane complex (IMC), facilitates the polarity and motility (Baum, 2006). *Plasmodium* motility is driven by an actin-myosin based motor that is anchored in the IMC (Baum, 2006). The distinctive shape of the ookinete is maintained by a twisted lattice of subpellicular microtubules that are associated with the IMC (Baum, 2006). These subpellicular microtubules are lined with proteins that stabilize and maintain the function of the microtubules. To date, very little is known about these microtubule associated proteins (MAPs) in *Plasmodium* ookinete biology. Some have been studied in the merozoite and sporozoite invasive stages and are primarily based on studies from related Apicomplexan parasites, such as *Toxoplasma gondii*.

Homology in a Related Apicomplexan Parasite, *Toxoplasma gondii*

Like *Plasmodium, Toxoplasma gondii* is a protozoan parasite and is a member of the phylum Apicomplexa. It is the causative agent of toxoplasmosis in humans. *T. gondii* replicates primarily in cats and can also survive in a variety of intermediate warm-blooded hosts, such as pigs and bird. *T. gondii* has been previously established as a good model for understanding Apicomplexan biology (Kim and Weiss, 2004; Baum et al., 2008). However, there are notable differences between *T. gondii* and *Plasmodium*. *Plasmodium* specifically infects hepatocytes and the red blood cells of its mammalian hosts, whereas *T. gondii* invades all nucleated cells and eventually infects many tissues, including the CNS, muscles, and placenta (Montoya and Liesenfeld, 2004). Additionally, while *T. gondii* is transmitted by contaminated food, water, infected faeces or tissues of warm blooded animals, *Plasmodium* is transmitted solely by mosquitoes. Keeping these distinct differences in mind, we can use the studies in *T. gondii* to a certain degree to inform our own hypotheses about *Plasmodium* biology.

Genes of Interest

trxl-1

As one of the major defense systems in *Plasmodium,* our lab studies the thioredoxin (trx) system and its potential cellular targets. We previously identified a novel *P. berghei* Thioredoxin-like protein, TrxL-1 (David *et al., in prep*) that is conserved across Apicomplexans where the closest *P. berghei* relative is *T. gondii* (Figure 3A) While the N and C terminus of TrxL-1 vary across species, there is a notably high level of conservation among the Trx-like domains (Figure 3B). Our initial biochemical characterization shows that the TrxL-1 protein is redox active and can interact with the thioredoxin system of *Plasmodium in vitro.* Despite its

redox activity, TrxL-1 shows very low levels of ROS reduction and therefore cannot be classified as an antioxidant enzyme.

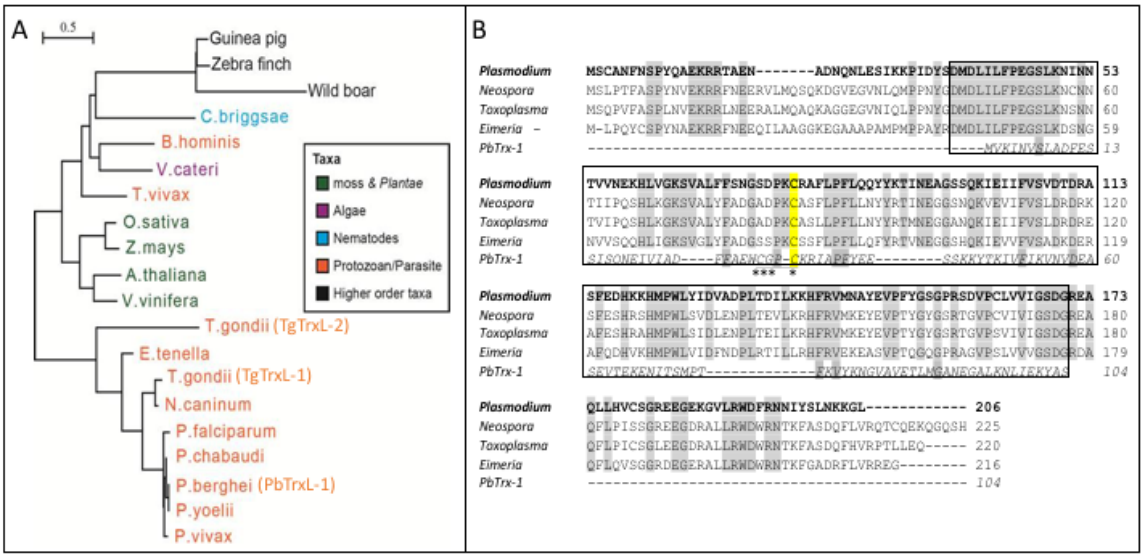

Figure 3 Conservation of PbTrxL-1. **(A)** Maximum likelihood tree using PhyML; alignments were done using CLUSTALW2 in Seaview. Bootstrapping with 100 replicates. The labels in parentheses indicate the previously described TrxL-2 and TrxL-1 of *Toxoplasma gondii* (Liu *et al*. 2013) and PbTrxL-1, respectively. **(B)** ClustalW alignment of TrxL-1 across the apicomplexan family with PbTrxL-1 in bold and PbTrx-1 for reference. Thioredoxin-like domain indicated by the black box. Asterisks denote the catalytic residues of PbTrx-1. Conserved redox active cysteine highlighted in yellow.

Characterization of the expression profile of *trxl-1* included RT-qPCR and was carried out by previous members of our lab (David *et al. in prep*). Relative transcript levels were examined in the blood stages and mosquito stages. The RT-qPCR data indicates that the *trxl-1* transcript is absent during parasite development in the mouse blood and highly upregulated during mosquito stage development (Figure 4A).

The data also reveals a 10-fold increase in *trxl-1* transcript abundance within the mosquito midgut when compared to the abundance in culture (Figure 4B). As the highest level of *trxl-1* transcript is observed during ookinete development, this suggests that *trxl-1* is involved in early mosquito stage development.

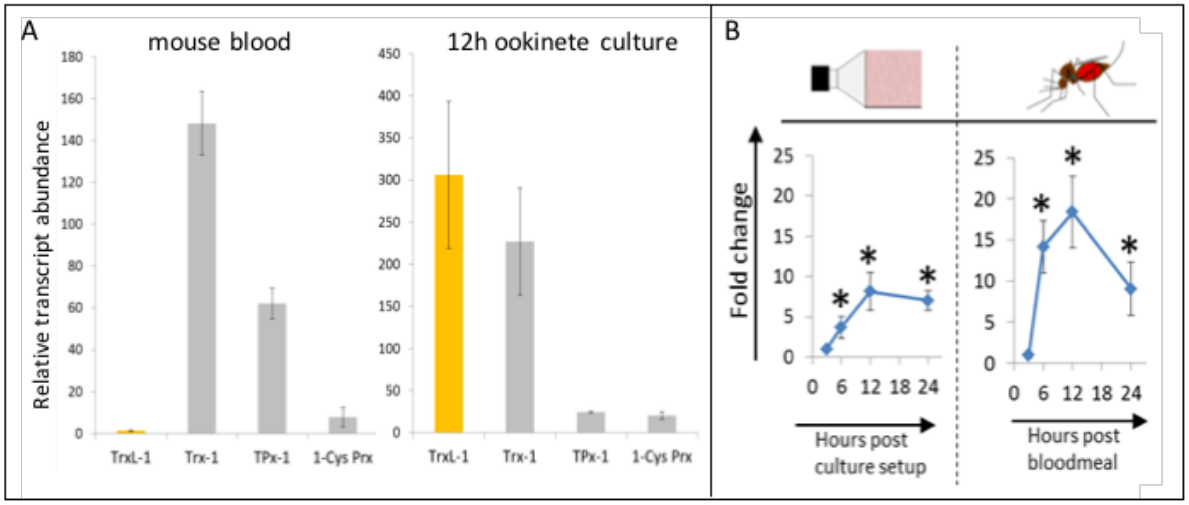

Figure 4 Stage Specific Expression of TrxL-1. (A) Relative transcript abundance of TrxL-1 in yellow compared to Trx-1, TPx-1, and 1-Cys Prx expression in grey. The RT-qPCR data indicates that there is no expression of TrxL-1 during asexual *Plasmodium* development in the mouse blood and TrxL-1 is highly upregulated during sexual stage development in the ookinete cultures. **(B)** Stage specific expression is evident in the mosquito as well. Compared to a 10 fold change in culture, TrxL-1 shows up to a 22 fold change within the mosquito midgut.

Notably, a recent study found that the *T. gondii* homolog, TgTrxL-1, is associated with subpellicular microtubules (Liu *et al.*, 2013). Futhermore, TgTrxL-1 localizes to the microtubules but does not directly affect microtubule stability. Because of our initial results on *trxl-1* and the findings in *T. gondii*, I decided to study the *Plasmodium trx-l* gene in this thesis.

spm-1

In the same *T. gondii* study described above (Liu *et al.* 2013), it was found that TgTrxL-1 indirectly interacts with the subpellicular microtubules via other proteins, prominently the subpellicular microtubule protein-1 TgSPM-1 (Tran *et al.*, 2012). Because of these findings, I also chose to study the *Plasmodium spm-1* gene in this thesis.

Unlike the mosquito specific expression of *trxl-1*, the expression profile data on *spm-1* taken from the *Plasmodium* genome database, PlasmoDB, shows an increase in transcript level during gametocytes (Aurrecoechea *et al*., 2009). Additionally, the SPM-1 protein contains a

conserved domain, the STOP (Stable Tubule Only Polypeptide) domain (Finn *et al.,* 2017). STOP proteins have been known to function as MAPs that are involved in the stabilization of axonemal microtubules by conferring cold resistance (Delphin *et al.,* 2012). An SPM-1 homolog, called STOP Axonemal protein-1 (SAXO-1), has been found to be involved in flagellum motility in another vector-borne protozoan parasite, *Trypanosoma brucei* (Dacheux *et al.,* 2012).

Using the data that our lab has accumulated on *trxl-1* together with the published data from the *T. gondii* studies on *spm-1*, **I hypothesize that *trxl-1* and *spm-1* play an important role in ookinete development, specifically in the stabilization of the subpellicular microtubule network**.

To investigate the cellular functions of *trxl-1* and *spm*-1, I decided to generate gene knockout (KO) parasite lines. However, most of the methods used to modify the *Plasmodium* genome are time-consuming and inefficient (Straimer *et al.* 2012). At the time that I started my thesis, the CRISPR/Cas9 system had just been used in *P. falciparum* (Wagner *et al.* 2014) and *P. yoelii* (Zhang *et al.,* 2014) to specifically edit these parasite genomes. Because of their success, I decided to adapt the CRISPR/Cas9 system to *P. berghei.*

CRISPR/Cas9 Genome Editing System

The CRISPR/Cas9 gene editing system has been developed as an efficient technology that can make precise changes to the genome. It has been successfully used to manipulate the genome of many organisms (Cong *et al.* 2013; Mali *et al.* 2013). It is based on Clustered Regularly Interspaced Short Palindromic Repeats (CRISPR) that act as a bacterial defense against invading viruses. CRISPR was transformed into a gene editing technology that can be used to target any locus of interest in the genome via an RNA-directed endonuclease, Cas9 (Figure 5). The small guide RNA (sgRNA) is co-transcribed and forms a complex with Cas9.

When the sgRNA aligns with its complement in the genome, Cas9 induces a double strand break (DSB) in the DNA. This DSB is either repaired with the nonhomologous end joining pathway (NHEJ) or homology directed repair (HDR).

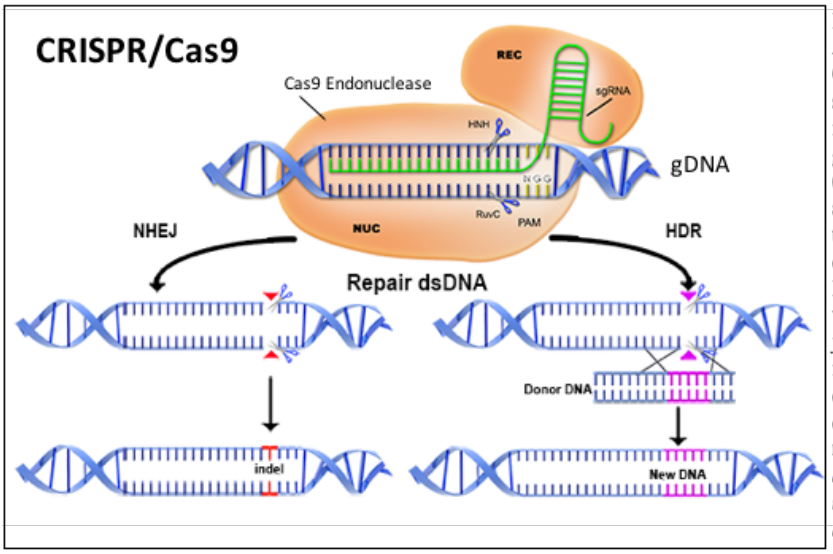

Figure 5 CRISPR/Cas9 System. An overview on the CRISPR/Cas9 gene editing system. The endonucleause Cas9 is directed to a specific site in the genome by a single guide RNA (sgRNA). When the sgRNA is aligned with it's complement in the genome, Cas9 induces a double strand break (DSB) in the DNA. The DSB can be repaired via the nonhomologous end joining pathway (NHEJ) resulting in a mutation or via homology directed repair (HDR) using a donor template to specifically modify the genome. *(Image adapted from https://www.aati-us.com/instruments/fragment-analyzer/crispr/)*

As this system enables the introduction of efficient, specific changes in any gene, it is an incredibly powerful and valuable tool for *Plasmodium* research. CRISPR/Cas9 has been previously established in other *Plasmodium* species, including the human parasite *P. falciparum* and the rodent parasite *P. yoelii.* (Wagner *et al.,* 2014; Zhang *et al.,* 2014) As CRISPR/Cas9 has not been established in the rodent model parasite *P. berghei,* I am the first to use this system in this malaria model. In this study, I investigated the function of two novel *P. berghei* genes via Cas9-mediated gene knockout.

Thesis Objective

Very little is understood about *Plasmodium* biology within the mosquito vector. The objectives of this project were to establish the CRISPR/Cas9 system in *Plasmodium berghei* and investigate the function of two novel mosquito specific genes, *trxl-1* and *spm-1.* The results presented in this thesis shed light on the molecular mechanisms that the malaria parasite utilizes

to survive in the mosquito and ultimately establish infection of the mosquito. While current malaria treatment and prevention strategies target the parasite in the human host, these data have the potential to inform novel transmission blocking strategies in the mosquito vector.

CHAPTER II

MATERIALS AND METHODS

Reagents

All PCR primers, oligos, enzymes, and corresponding enzyme buffers were obtained from Thermo Fisher Scientific (Waltham, MA).

Amresco; Solon, OH: glycerol, sodium dodecyl sulfate (SDS), tris.

Bioexpress; Kaysville, UT: 10X phosphate buffered saline (PBS), agar, fetal bovine serum (FBS), nuclease free water, tryptone, urea.

Growcells.com; Irvine, CA: X-Gal Powder.

Lonza; Basel, Switzerland: Nucleofector Kit T.

Molecular Research Center, Inc.; Cincicannati, OH: Tri-Reagent RT.

Open Biosystems; Huntsville, AL: anti-Thioredoxin rabbit serum.

Promega; Madison, WI: dithiothreitol (DTT), JM109 Competent Cells, pGEM-T Easy Vector System.

Sigma-Aldrich; St. Louis, MO: ethylenediaminetetraacetic acid (EDTA), Giemsa, Heparin sodium salt, nycodenz, paraformaldehyde, penicillin-streptomycin, phenylhydrazine, proteinase K, pyrimethamine, RPMI-1640 medium, saponin, triton X-100, tween 20.

Southern Biotech; Birmingham, AL: DAPI Fluoromount-G.

Thermo Fisher Scientific; Waltham, MA: 6X DNA Loading Dye, Alexa Fluor 488 Goat anti-Rabbit IgG, Alexa Fluor 555 Goat anti-Mouse IgG, ampicillin trihydrate, bovine serum albumin (BSA), boric acid, dimethyl sulfoxide (DMSO), DreamTaq PCR Master Mix, Ethidium Bromide Solution, GeneJET Gel Extraction Kit, GeneJET Whole Blood Genomic DNA Purification Mini Kit, GeneJET PCR Purification Kit, GeneJET Plasmid Miniprep Kit, GeneRuler 1 kb Plus DNA Ladder, glacial acetic acid, glycine, hydrochloric acid (HCl), isopropyl β-D-1-thiogalactopyranoside (IPTG), methanol, magnesium chloride ($MgCl_2$), potassium phosphate (KH_2PO_4), sodium borohydride,

sodium chloride (NaCl), sodium hydroxide (NaOH), sodium phosphate (Na_2PO_4), TopVision LE GQ Agarose, yeast extract.

Whatman; Dassel, Germany: Reinforced Nitrocellulose Membrane.

Buffers, Media, and Solutions

10X TBE Electrophoresis Buffer: 108 g Tris base, 55 g boric acid, 40 mL 0.5 M EDTA (pH 8.0), dH_2O to 1L.

Freezing medium (blood stocks) 20% Glycerol: 10 mL glycerol, 5 mL 10X PBS, 35 mL nuclease free water. Filter sterilize.

Freezing medium (bacterial stocks) 50% Glycerol: 25 mL glycerol, 5 mL 10X PBS, 20 mL nuclease free water. Filter sterilize.

50X TAE Electrophoresis Buffer: 242 g Tris base, 57.1 mL glacial acetic acid, 100 mL 0.5 M EDTA (pH 8.0), dH_2O to 1L.

Blocking Buffer: 3% BSA in PBST.

Luria-Bertani (LB) Medium: 5 g yeast extract, 10 g NaCl, 10 g tryptone, 1L dH_2O. Sterilize by autoclaving.

Ookinete Culture Medium: RPMI-1640, 20% FBS, 1% pen-strep, pH 8.2. Filter sterilize.

PBST: 1X PBS, 0.1% Tween 20, pH 7.2. Sterilize by autoclaving.

Pyrimethamine Solution (7mg/mL): 70 mg pyrimethamine, 10 mL DMSO. Dissolve pyrimethamine in DMSO via vortexing. Dilute 100X with tap water for final volume of 1L. Adjust pH to 3-5. Store at 4 degrees for 7-10 days.

Shizont Culture Medium: RPMI-1640, 20% FBS, 1% pen-strep, pH 7.2. Filter sterilize.

Accession Numbers

Protein Name	PlasmoDB Accession Number
Thioredoxin 1 (Trx1)	PBANKA_1320900
Thioredoxin Reductase (TrxR)	PBANKA_0824700
Thioredoxin-like Protein-1 (TrxL1)	PBANKA_0820200
Subpellicular Microtubule Protein 1 (SPM1)	PBANKA_0810700
1-Cysteine Peroxiredoxin (1-Cys Prx)	PBANKA_122800

Table 1. Accession numbers for all genes examined.

Ethics statement

All experimental protocols followed the National Institutes of Health guidelines for animal housing and care and were approved by the Institutional Animal Care and Use Committee (IACUC) of Loyola University Chicago (Protocol#1429/40).

Parasite Maintenance

Plasmodium berghei ANKA 2.34 wild type (WT) parasites were maintained in outbred Charles River strain CF1 mice. After a maximum of six passages, the parasites were passed through *Anopheles stephensi* mosquitoes and subsequently kept at 19°C, 80% RH, 12 hrs light-dark cycle, 5%glucose solution. On day 17 post infectious blood meal (PIBM), the mosquitoes were allowed to feed on naïve mice for 15 minutes. The new generation of parasites were harvested when the mice reached ~30% parasitemia (percent infected RBCs). Blood stocks of *P. berghei* parasites were stored at -80°C in 20% glycerol in phosphate-buffered saline (PBS).

Mosquito Maintenance

Anopheles stephensi mosquitoes were reared under standard conditions in the insectary (26°C, 80% RH, 12 hrs light-dark cycle). The mosquito colony was maintained by allowing one bucket of at least one week old mosquitoes to feed on mice once a week. Two days post feed, an egg cup was placed in the bucket where the female mosquitoes lay their eggs and three to six new pans were set to equilibrate. Three days post feed, eggs from the egg cup were transferred to the equilibrated pans. Larvae were fed daily until pupation. All mature pupae were transferred to a new bucket in a small cup. Once the pupae emerged, the mosquitoes were provided with a 5% glucose feeding solution in a cup with filter paper.

Exflagellation

The egress and subsequent exflagellation of the male gametocytes is measured *in vitro* via live bright field microscopy. 2 uL of infected mouse tail blood is incubated in 2 uL heparin and 50 uL ookinete culture medium at 19°C for 15 minutes. 10 uL of each sample is added under the cover slip of a hemocytometer. The number of exflagellating cells are counted per 20X field.

Ookinete Cultures

For the enrichment of gametocytes, mice were pretreated with phenylhydrazine (Phz) 2 days before injecting blood stage parasites. Exflagellation rates were checked 2 days post-infection. The blood was harvested when exflagellation reached >10 exflagellations/20X field. The blood of infected mice was pooled, diluted 1∶5 with ookinete culture medium (RPMI-1640, pH 8.2), and incubated at 19°C for 24 hrs.

Infectious Mosquito Feeds

Similar to the ookinete cultures, mice were pretreated with phenylhydrazine (Phz) 2 days before injecting blood stage parasites. Exflagellation rates were checked 2 days post-infection. Once the exflagellation reached >10/20X field, female *Anopheles stephensi* mosquitoes were allowed to feed on the infected mice for 15 minutes. The bloodfed mosquitoes were subsequently stored in an environmental chamber kept at 19°C, 80% RH, 12-hour light-dark cycle, 5% glucose solution.

Isolation and Purification of *P. berghei* genomic DNA

Genomic DNA (gDNA) was extracted from 200 uL of whole blood of the infected mice. The GeneJET Whole Blood Genomic DNA Purification Mini Kit was used to perform cell lysis and subsequent DNA purification. DNA concentration and purity was assessed using the

FLUOstar Omega plate reader (*BMG Labtech; Cary, NC*). All gDNA samples were stored at -20°C.

CRISPR/Cas9 design and Plasmid Construction

The TrxL-1 KO and SPM-1 KO plasmids were generated using the plasmid pYC (for plasmid for *yoelli* containing Cas9) which was a kind gift from Jing Yuan, Xiamen University, Xiamen, Fujian, China. The PyU6 promoter driving the sgRNA cassette was replaced with a *Plasmodium berghei* specific U6 snRNA promoter (PbU6) that was amplified from *P. berghei* ANKA genomic DNA (Primers in Table 2). The *P. berghei* specific plasmid was named pBC (plasmid for *berghei* containing Cas9).

The 20bp target sequence (TS) for each gene of interest was determined using Geneious 8 (https://www.geneious.com, Kearse et al., 2012). The annealed oligonucleotide TS for *trxl-1* was inserted into the BsmBI restriction site. Due to difficulties in the ligation of the *trxl-1* TS, the *spm-1* TS was designed into the forward primer of a primer set that amplified the sgRNA using pBC as the template. The resulting *spm-1* TS-sgRNA product was inserted into pBC and replaced the empty sgRNA scaffold.

For the generation of a targeted and easily detectable gene deletion, a homology template for Homology Directed Repair (HDR) of each gene of interest was designed in the pCR4-TOPO TA Vector (a generous gift from Kim Williamson, Uniformed Services University) based on previously described methods [3]. The 5' and 3' genomic regions flanking each gene of interest were amplified from PbWT genomic DNA and successively inserted on each side of a short disrupter. The complete 5'UTR-Disrupter-3'UTR homology construct was inserted into the HindIII restriction site on pBC. The finished TrxL-1 KO plasmid was named pBCT (plasmid for

berghei containing Cas9 for *trxl-1* KO) and the SPM-1 KO plasmid was named pBCS (plasmid for *berghei* containing Cas9 for *spm-1* KO).

Polymerase Chain Reaction (PCR)

All PCR reactions were incubated on the Eppendorf Mastercycler ep gradient S thermal cycler. The primers used for the amplification of the PbU6 promoter, TrxL-1 5' UTR and 3' UTR, SPM-1 5' UTR and 3' UTR, TrxL-1 target sequence, SPM-1 target sequence and guide RNA, gene disrupter, and sequencing reactions are listed in Table 2.

Target	Fwd	Primer Sequence 5' → 3'	Rev	Primer Sequence 5' → 3'	Amplicon
PbU6	P1	GGCGCCCTCTACTTCACGCAAATGTAACAC	P2	CATATGTATAACTCGAAGTATGCGCATATG	337 bp
TrxL1 5' UTR	P3	GGATCCGCAAGCTTGGATGTGTTAAGTGTATTATGGATGGC	P4	GGATCCCCATTTAAACTATTATGTTC	359 bp
TrxL1 3' UTR	P5	TCTAGAACATATTTGCCAATGTGGAGAACG	P6	TCTAGAGCAAGCTTCTTATACTTTATTTCATCCC	361 bp
SPM1 5' UTR	P7	GGATCCGCAAGCTTAACATTTTACAGAAATATGCAGC	P8	GGATCCCATCTATGAAAGCCACACGT	690 bp
SPM1 3' UTR	P9	TCTAGACAGCTGAACATATATTTTGGG	P10	TCTAGAGCAAGCTTATACGTGCATTTCTTAGCGTTTCC	497 bp
Sequencing Homology Constructs	P11	AATTTCACACAGGAAACAGC	P12	GCACAATATCTAGGATACTAC	-----
TrxL1 TS	P13	GTTTTTAGTCGTTATCGGAAGTGA	P14	AAACTCACTTCCGATAACGACTAA	-----
SPM1 TS-sgRNA	P15	TCAGCTGGATAAGTAGGTGCGTTTTAGAGCTAGAAATAGCAAG	P16	TGACGTCCAAAAAAAGCACC	150 bp
Gene Disrupter	P17	GGATCCACTAGTAACGGCCG	P18	GCTAGCTACGAAGGGCGAAT	-----
Sequencing TrxL1	P19	TTGCTAATTTTTTGTGAGCAGACC	P20	CAATCGCACATGCACGTATTCG	-----
Sequencing SPM1	P21	GACTGTTTATTTTAAAGCACATTG	P22	GCATAATTCATTCAATCGATTTCC	-----

Table 2. PCR Primers.

All reactions were set up using the general guidelines as follows:

5 uM forward primer,
5 uM reverse primer,
750 ng gDNA template,
1X DreamTaq PCR Master Mix
Nuclease free water up to a final volume of 20 uL

All reactions were incubated in the ThermoCycler with the following program:

Initial Denaturing: 10 minutes at 95°C

Denaturing: 30 seconds at 95°C
Annealing: 30 seconds at 56°C - 60°C
Elongation: 30 seconds – 3 min at 72°C
} 35 Cycles

Final Elongation: 5 minutes at 72°C

The primer annealing temperature was determined first by subtracting 5 degrees from the melting temperature provided. If the reaction did not work, a gradient was set up to determine optimal annealing temperature for the primer sets. The elongation time was determined by the length of the desired PCR product following the convention that the polymerase runs at about 1 kb per minute.

If the gradient did not prove successful, the concentration of magnesium chloride was increased due to the difficult template. Increasing magnesium chloride concentration improved the genomic DNA amplification where there is a high AT content.

DNA Electrophoresis

Depending on their size, all DNA fragments were run out on a 0.8% - 1.2% agarose gel containing 0.5 ug/mL ethidium bromide. If the samples did not already contain loading dye, 6X DNA loading dye was added to a final concentration of 1X. GeneRuler 1 kb Plus DNA Ladder was used to determine DNA fragment size. The gel was run in 1X TAE buffer at 110V for 40 minutes using the Owl Horizontal Gel Electrophoresis System (Thermo Fisher Scientific; Waltham, MA). The DNA bands were visualized under UV light and subsequently extracted with the GeneJET Gel Extraction Kit.

TA Cloning of PCR Products into pGEM

The pGEM-T Easy Vector System II was used with the gel extracted PCR products. The reagents were used in the following concentrations: 1X Rapid Ligation Buffer, 25 ng pGEM-T Easy Vector, 3 units T4 DNA Ligase, PCR product 3-5 times more concentrated than the vector, and nuclease free water up to 10 uL. The ligation was incubated overnight at 4°C.

Transformation of JM109 *E. coli* Competent Cells

2 uL of a ligation mixture was gently mixed with 25 uL of competent cells in a 1.5 mL microcentrifuge tube. The cell-ligation mixture was incubated on ice for 20 minutes. The cells were heat shocked at 42°C for 45 seconds and placed on ice for 2 minutes. 275 uL of LB medium was added to the cells and incubated in a shaking incubator at 37°C for 1 hour. The resulting transformed cells were spread on pre-warmed LB/agar plates containing 0.1 mg/mL ampicillin.

If transforming a pGEM ligation, blue/white screening was also used. Before addition of the transformed cells, 0.1 mM IPTG and 20 ug/mL X-Gal was spread onto the LB/agar plates and allowed to absorb. Once the cells soaked into the plate, the plate was inverted and incubated at 37°C overnight.

Restriction Digests

Restriction digests for each desired fragment were set up using the enzymes listed in Table 3. The reactions were set up according to the manufacturer's instructions using each enzyme's recommended buffer. The digests were incubated for at least 2 hours (up to overnight) at 37°C and subsequently run out on a 0.8% - 1.2% agarose gel. If a fragment was to be inserted into a vector, the digested vector was dephosphorylated using a Calf Intestinal Alkaline

Phosphatase (CIAP) before running the sample on the gel. The correctly sized DNA fragments were cut out and purified via gel extraction.

Primer Set	Forward	Reverse	Fragment Size
PbU6	KasI	NdeI	337 bp
TrxL1 5' UTR	BamHI, HindIII	BamHI	359 bp
TrxL1 3' UTR	XbaI	XbaI, HindIII	361 bp
SPM1 5' UTR	BamHI, HindIII	BamHI	690 bp
SPM1 3' UTR	XbaI	XbaI, HindIII	497 bp
SPM1 TS-sgRNA	NdeI	AatII	150 bp

Table 3. Restriction Enzymes.

Ligations of DNA Fragments into a Vector

Ligations into vectors other than pGEM were set up using 1X T4 DNA Ligase Buffer, 1 unit T4 DNA ligase, and varying ratios of insert to vector where there was always at least 2X more insert than vector. The reaction was incubated at room temperature for 2 hours or overnight at 4°C.

DNA Isolation, Purification, and Concentration

Precultures with transformed bacterial colonies were set up with 1 colony in 5 mL LB medium and 5 uL of 100 mg/mL ampicillin. The precultures were incubated overnight in a 37°C shaker and pelleted the following day. Plasmids were isolated from the bacteria and purified using the GeneJET Plasmid Miniprep Kit. If necessary, the plasmid DNA was precipitated and concentrated using ethanol. 0.1 volumes of 3M sodium acetate and 3 volumes of ice cold 100% ethanol was added to the DNA and mixed via vortexing. The DNA was allowed to precipitate for at least 1 hour at -20°C and pelleted at 13000 rpm at 4°C for 30 minutes. The pellet was washed twice with 500 uL ice cold ethanol and spun down at 4°C for 10 minutes after each wash. The

ethanol was carefully removed and allowed to dry. The pellet was resuspended in an appropriate volume of nuclease free water.

Generation of Transgenic Parasites

All transgenic parasite lines were generated from *Plasmodium berghei* ANKA wild type (PbWT) parasites. Each plasmid (pBC, pBCT, and pBCS) was transfected following previously described methods (Janse et al., 2006).

Schizont Culture and Purification

A naïve mouse was infected with PbWT parasites from a frozen blood stock. The infected mouse was then exsanguinated and passed into 2-4 new mice. When the mice reached a parasitemia of 1-3%, they were exsanguinated and the blood was added to 10 mL of schizont culture medium supplemented with heparin. The blood was spun down at 500xg slowly and the supernatant was discarded. The blood was resuspended in fresh schizont culture medium and transferred to tissue culture flasks. The cultures were incubated overnight at 37°C with 5% CO_2 and 3% O_2.

The cultures were harvested when around 80% of the schizonts were mature with 8-14 merozoites per cell. The blood was gently layered on top of a 17% Nycodenz layer and centrifuged slowly at 500xg for 20 minutes. The interface between the layers that contains the mature schizonts was collected with a Pasteur pipet, transferred to a fresh tube, and supplemented with fresh culture medium. The collected schizonts were again centrifuged at 500xg for 10 minutes. The supernatant was removed, and the pellet was resuspended in enough media to aliquot 1 mL of resuspended schizonts per 1 injection. The aliquoted schizonts were

briefly centrifuged for 5 seconds at 17,000xg. The supernatant was removed and the pellet was immediately used for transfection.

Transfection of *P. berghei*

The plasmids were transfected into *P. berghei* schizonts using the Nucleofector kit T (VCA-1002; Lonza, MD). 80 uL of the Nucleofector Solution and 20 uL of the Nucleofector Supplement were added to 10 uL of linearized plasmid DNA at a concentration of .5 - 1 ug/uL. 100 uL of the DNA mixture was used to resuspend 1 pellet of aliquoted schizonts. This cell suspension was quickly transferred to an electroporation cuvette and inserted into the Amaxa Nucleofector I Electroporator (Amaxa Biosystems; Cologne, Germany). Electroporation was carried out using program U33.

Immediately following electroporation, the cells were supplemented with 50 uL of fresh pre-warmed schizont culture medium. The 150 uL of transfected cells was then directly injected into the tail vein of naïve mice using an insulin syringe. The mice were positioned under a heat lamp 5-10 minutes prior to injection in order to increase the size and visibility of the veins in the mouse tail.

Drug Selection

The transfected constructs all contain a pyrimethamine resistance gene, *dhfr*. In order to select for the transgenic parasites, pyrimethamine was added to the drinking water 1 day after the injections. Around 8-10 days post injection, the pyrimethamine-resistant parasites could be visualized in the blood. The blood containing transgenic parasites was harvested and the genomic DNA was extracted.

Verification of Gene Knockout

CRISPR/Cas9 mediated gene deletion was verified via PCR using specific primers up and downstream of the genomic region coding for each gene. The primers were located outside of the region amplified for the generation of the homology construct on the plasmids to ensure that there was no cross reactivity with the transfected plasmid.

Parasite Cloning

PCR verified KO parasites were passed into naïve mice for cloning. 2 uL of tail blood from the infected mice was diluted so that 1 parasite was injected intravenously into 6 naive mice. The cloned parasite lines were then used in all subsequent experiments and analyses.

Growth Curves

Blood Stages

For the analysis of growth in the blood stages, a predetermined number of parasites were injected directly into the tail vein of naïve mice. After the injection, the mice were monitored daily with blood smears. The blood was taken from a tail snip, smeared, fixed with methanol, and stained with Giemsa. The parasitemia was measured daily until the mice showed signs of illness. The mice were then exsanguinated and the blood was stored at -80°C.

Mosquito Stages

In order to assess ookinete development *in vitro*, ookinete cultures were set up. At 12, 18, and 24 hours post culture set up, samples of the cultures were smeared, fixed with methanol, Giemsa-stained, and visualized with light microscopy at 100X magnification. The ookinetes were classified as either mature or immature based on the level of development for each time point.

In order to assess ookinete development *in vivo,* infectious mosquito feeds were set up. At 12, 18, and 24 hours post infectious blood meal (PIBM), bloodfed mosquito midguts were dissected. Each midgut was resuspended in 5 μL of PBS and smeared on a slide. Each slide was fixed in methanol, stained with Giemsa, and visualized with light microscopy at 100X magnification. The ookinetes were classified as either mature or immature based on the level of development for each time point.

Sampling and Fixation of Parasites

Blood stage parasites were isolated from tail vein blood from mice and were resuspended in RPMI-1640 pH 7.4 media with heparin pre-warmed to 37°C and allowed to adhere to 0.01% poly-L-lysine coated glass slides at 37°C. Gametogenesis was induced by resuspending tail blood in RPMI-1640 pH 8.2 media with heparin pre-warmed to 19°C and allowed to adhere to 0.01% poly-L-lysine coated glass slides at 19°C. Cells were then fixed in 3% paraformaldehyde with 0.1% glutaraldehyde at 4°C. Cultured ookinetes were taken at experimental time points 12, 18, and 24 hours post culture setup. RBCs were lysed with 0.17 M NH4Cl. Cells were then resuspended in 0.05 M Tris 0.9% NaCl pH 8.2 and allowed to adhere to 0.01% poly-L-lysine coated glass slides. Cells were then fixed in 4% paraformaldehyde at 4°C. Midgut ookinetes were isolated from dissected midguts by crushing midguts with mortar and pestle in 0.05 M Tris 0.9% NaCl pH 8.2 and allowed to adhere to 0.01% poly-L-lysine coated glass slides.

Immunofluorescence Labeling

All steps were carried out at room temperature unless stated otherwise. Prepared slides were permeabilized with 0.1% Triton-X and blocked with 3% Bovine Serum Albumin (BSA) in PBS containing 0.1% Tween-20 (PBST). Slides were incubated overnight at 4°C with rabbit

polyclonal anti-sera containing anti-PbTrx-1 antibodies (diluted 1:500 in blocking buffer) and mouse monoclonal antisera containing anti-α-tubulin antibodies (diluted 1:2000). Slides were then incubated for 1 hour with goat anti-rabbit or anti-mouse IgG Alexa Fluor 488 or 555, respectively, (generous gifts from Dr. Tom Sanger and Dr. Jennifer Mierisch, Loyola University Chicago) diluted 1:1000 with blocking buffer. Slides were sealed with glass cover slips in DAPI mounting medium.

Sequence Alignments

Geneious v8 (Kearse *et al.*, 2012) was used to compile all sequences that were aligned. The alignments were performed via MUSCLE within the Geneious software. The protein sequence features were determined using the InterPro database (Mulder *et al.*, 2005).

Statistical Analysis

For the blood stage growth curves, statistically significant differences were determined using independent t-tests using GraphPad Prism version 7 for Mac, GraphPad Software, La Jolla California USA www.graphpad.com. For the mosquito stage growth curves, statistically significant differences were determined using independent t-tests using R version 3.3.1 Vienna, Austria http://www.R-project.org. The level of development (mature vs. immature) of the WT and TrxL1 KO ookinetes were compared at each time point.

CHAPTER III

RESULTS

Establishing the CRISPR/Cas9 System in *Plasmodium berghei*

In order to successfully establish and utilize the CRISPR/Cas9 system in *P. berghei,* I created a new protocol using online resources and previous literature as a guide (Wagner *et al*. 2014; Zhang *et al.* 2014; Addgene.org). I studied the CRISPR information available on the nonprofit plasmid repository, Addgene, to learn how to adapt the CRISPR/Cas9 technology to *P. berghei*. To generate an effective working protocol and inform my experimental design, I specifically used Addgene's CRISPR tools, such as the CRISPR guide and the CRISPR 101 eBook.

Generation of the CRISPR/Cas9 Specific Plasmid

As researchers had recently established the CRISPR/Cas9 system in *P. falciparum* (Wagner *et al*. 2014) and *P. yoelii* (Zhang *et al.* 2014), I investigated the possibility of using their constructs as templates. The establishment of CRISPR in *P. falciparum* required the co-transfection of two plasmids, one containing the Cas9 construct, and the other containing the replacement cassette for the target gene (Wagner *et al.,* 2014). This significantly decreases the efficiency of transfection and production of transgenic parasites. In contrast, the *P. yoelii* plasmid pYC contains all of the necessary CRISPR/Cas9 components on one large plasmid (Figure 6) (Zhang *et al.,* 2014). pYC is comprised of a strong constitutive *P. berghei elongation factor 1 alpha* promoter (*Pbef1α)* that drives the expression of the CRISPR-associated endonuclease

(Cas9) gene as well as a *P. yoelii* U6 small nuclear RNA promoter (PyU6) that drives the expression of the single guide RNA (sgRNA) scaffold. pYC also contained two drug resistance genes, an ampicillin resistance gene for plasmid selection in *E. coli* and a pyrimethamine resistance gene for selection of transgenic parasites. Because pYC was shown to be successful in establishing CRISPR in *P. yoelii* (Zhang *et al.* 2014) and only required the transfection of one construct, I decided to use pYC as my template. Following an inquiry with Dr. Jing Yuan from the Xiamen University in Xiamen, China, I received pYC as a generous gift.

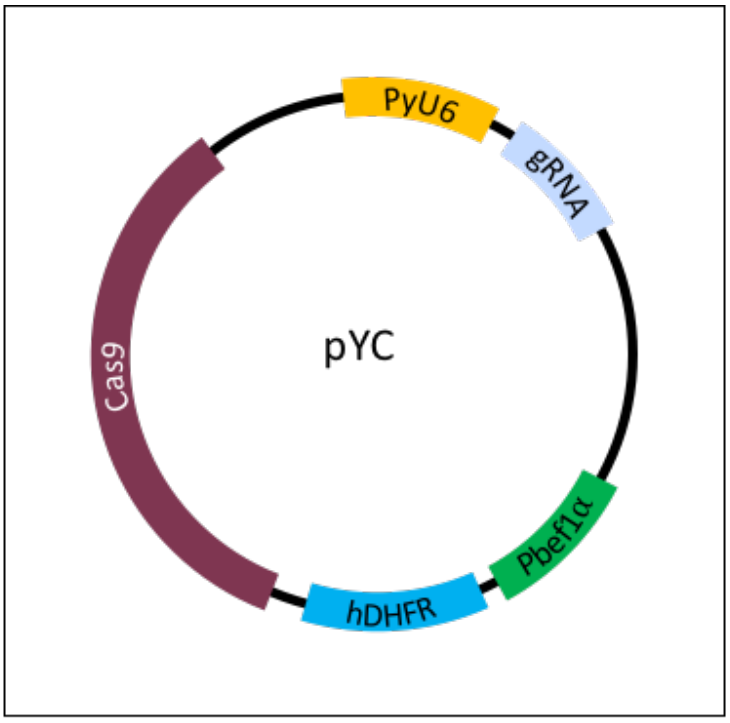

Figure 6 Organization of pYC. pYC contains a *P. yoelii* U6 promoter (PyU6), the guide RNA scaffold (gRNA), the *P. berghei* elongation factor 1α promoter (Pbef1α), the pyrimethamine resistance gene (hDHFR), and the CRISPR-associated nuclease gene (Cas9).

To make the CRISPR plasmid specific to *P. berghei*, I first needed to replace the *P. yoelii* U6 promotor with the homologous *P. berghei* U6 promoter. Using the BLAST sequence alignment too (Altshul *et al.* 1990), I searched the *P. berghei* genome for similar RNA promoters

and found an annotated *P. berghei* U6 spliceosomal RNA homolog (Otto *et al.,* 2014). To clone the promoter (PbU6), I designed primers and amplified a 340 bp segment upstream of the transcription start site of the U6 homolog. Following sequence verification, I replaced PyU6 in pYC with the PbU6 to function as the new *P. berghei* specific promoter. I named the resulting plasmid, pBC (plasmid for *P. berghei* CRISPR/Cas9), which was used for all future modifications described herein.

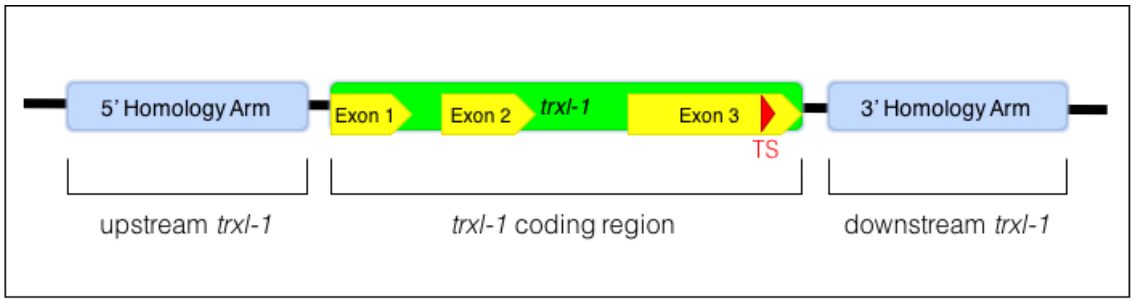

Figure 7 Organization of the *trxl-1* Genomic Region. To generate the *trxl-1* homology construct, regions upstream and downstream of the *trxl-1* coding sequence were used as the 5' and 3' homology arms, respectively. The target sequence (TS) used for the Cas9-mediated gene deletion is located near the 3' end of exon 3 (shown in red).

The next step was to modify pBC to generate a *trxl-1* knockout plasmid. I first identified a 20 bp target sequence (TS) within the *trxl-1* gene (Figure 7) that ended with a PAM sequence of 5' NGG 3'. In order to identify the best candidates for the TS, I utilized the *'Find CRISPR sites'* function in the sequence analysis software, Geneious v8 (Kearse *et al.*, 2012). It scans the gene of interest, cross references it to the *Plasmodium berghei* genome, and scores each 20 bp sequence with a specified PAM sequence of 5' NGG 3'. The score is generated based on the nucleotide composition, type of PAM sequence (TGG is preferred), and the number of potential off-target sites in the genome. 100% is the maximum CRISPR score possible.

From the scored sequences in the *trxl-1* CDS, I chose a TS within exon 3 that resulted in a CRISPR score of 99.96% (TS location shown in figure 7). The short nature of the TS allowed

me to design it as two overlapping oligonucleotides with flanking restriction sites. I next attempted to clone the 20 bp TS into pBC. However, this proved to be inefficient as sequencing revealed that multiple copies of the TS were inserted sequentially into the plasmid (Figure 8 LEFT).

I repeated the cloning process while varying the concentration of the TS and sequenced the resulting plasmids. After three rounds of cloning and sequencing, I finally detected one bacterial colony containing a plasmid with only one copy of the 20 bp TS inserted directly upstream of the sgRNA (Figure 8 RIGHT). I named the resulting plasmid pBCT (plasmid for *P. berghei* CRISPR/Cas9 mediated trxl-1KO).

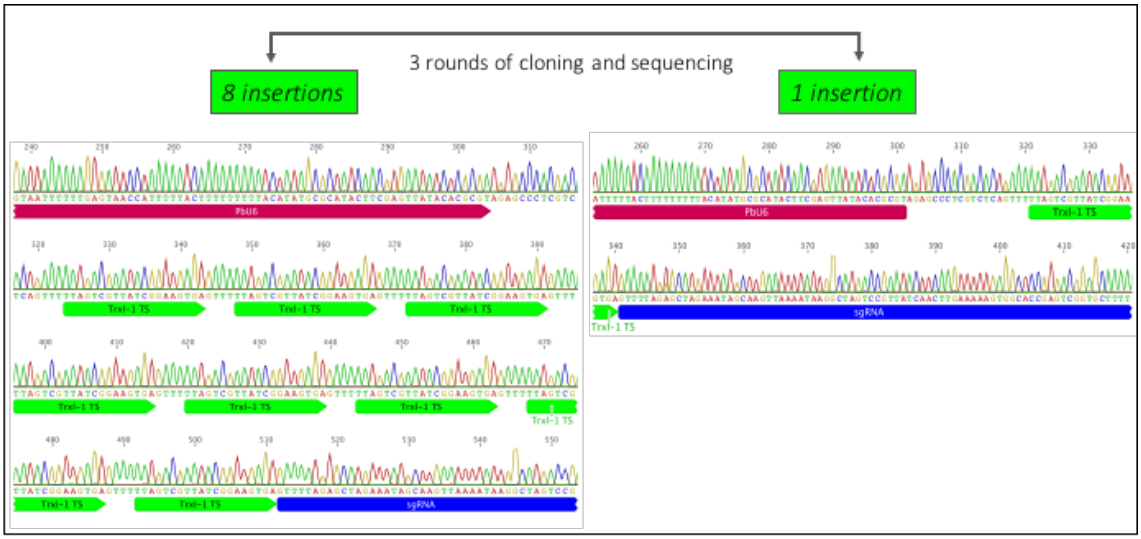

Figure 8 Cloning of the *trxl-1* TS. Sequencing results representative of the first two attempts of cloning the 20 bp TS (green) where it inserted 7-12 times (LEFT). The third attempt resulted in the desired sequence with a single insertion. PbU6 marked in red and sgRNA marked in blue (RIGHT).

For an additional level of specificity, I next designed a *trxl-1* homology construct to act as a donor template for the homology directed repair (HDR) of the Cas9-induced double strand break (DSB) (See Figure 3). I generated the left and right homology arms by cloning 300-500 bp regions upstream and downstream of the *trxl-1* coding region, respectively. In a separate vector, I

designed the construct around a short, random gene disrupter (IN) where the disrupter sequence is flanked by the right and left homology arms (Figure 9).

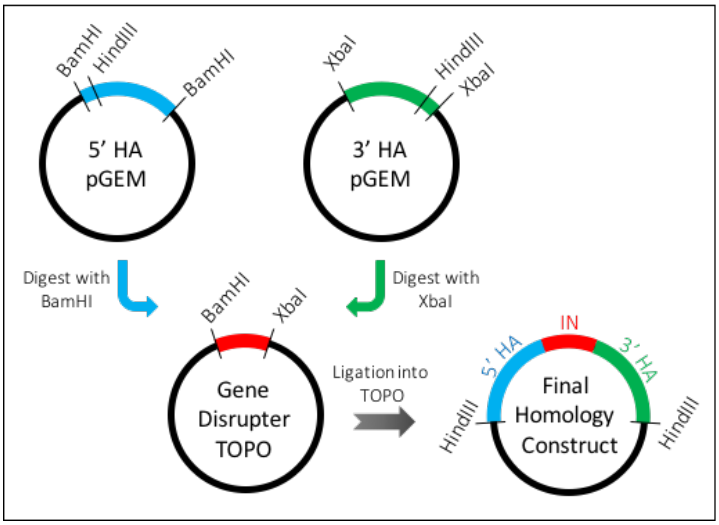

Figure 9 Generation of Homology Construct. The homology construct for each gene was designed around a small, random gene disrupter (IN) inserted in to the TOPO vector. The 5' and 3' homology arms (HA) were cloned into pGEM and digested with BamHI and XbaI, respectively. The 5' HA and 3' HA were ligated into the TOPO vector sequentially to generate the complete homology construct. The final homology construct was cloned out using dual HindIII restriction sites and ligated into the final plasmid, pBC (not shown).

The homology construct was excised and cloned into pBCT, completing my *trxl-1KO* CRISPR plasmid. pBCT, contains all of the required machinery to adapt the CRISPR/Cas9 system to *Plasmodium berghei* and generate a targeted gene knock out of *trxl-1*.

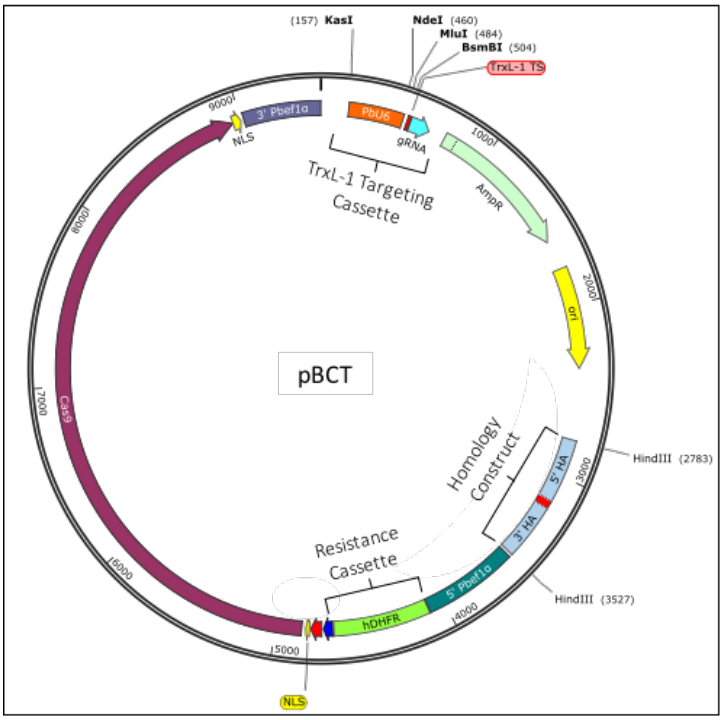

Figure 10 Plasmid Map of pBCT. Generated plasmid map showing all of the necessary elements of the TrxL-1 KO plasmid, pBCT. It contains a *P. berghei* U6 promoter (PbU6) driving expression of the *trxl-1* target sequence (TrxL-1 TS) and the guide RNA (gRNA), a *P. berghei* promoter (Pbef1α) driving the expression of the pyrimethamine resistance gene (hDHFR) and the 2A FLAG-Cas9 gene, a *trxl-1* homology construct with both 5' and 3' homology arms (HA), and an ampicillin resistance gene (AmpR). Map generated with SnapGene software (GSL Biotech).

A plasmid map detailing all genetic elements of pBCT is shown in Figure 10. I have also included a simplified schematic demonstrating how pBCT serves as the template during HDR (Figure 11).

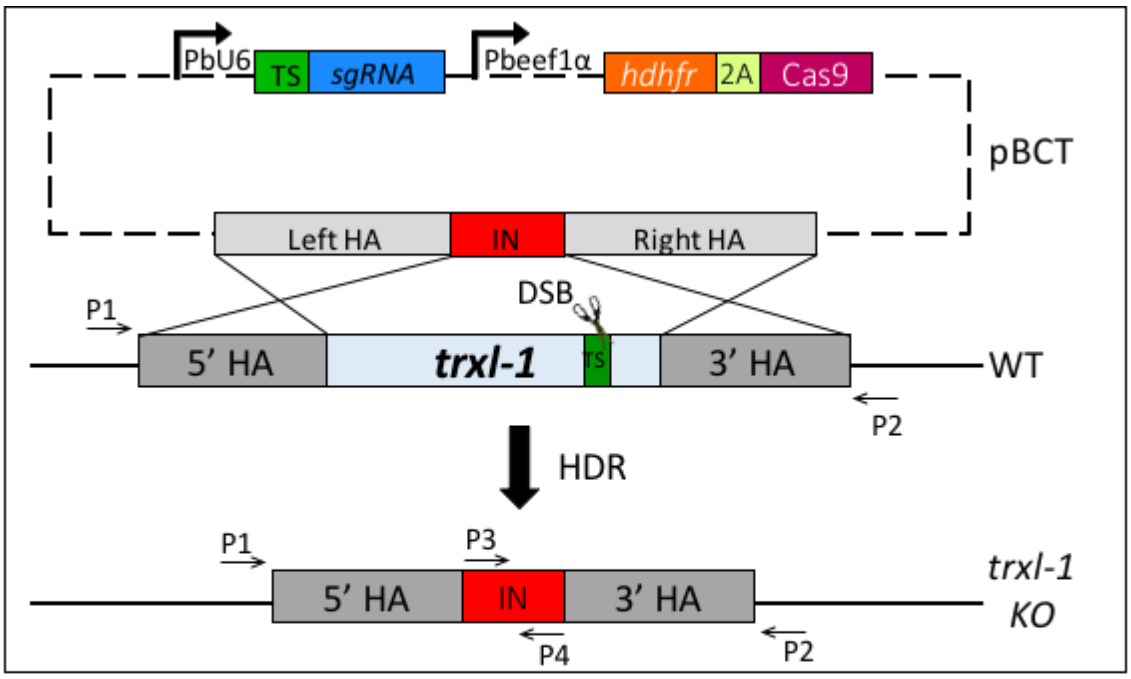

Figure 11 Schematic of pBCT as the Donor Template for HDR. Following the Cas9-induced double strand break (DSB), the *trxl-1* homology construct acts as a template for homology directed repair (HDR). Within the homology construct on pBCT, a small disrupter sequence (IN) is flanked by the left and right homology arms. Following a double crossover event, the disrupter replaces the *trxl-1* gene and PCR primers (P1-P4) are used to detect successful gene knockout.

Generation of Transgenic *P. berghei*

To generate *trxl-1KO* parasites, pBCT was prepared for transfection. The blood of *P. berghei* WT-infected mice was harvested at a 1-3% parasitemia. The parasites were cultured overnight to allow them to mature into schizonts. The schizonts were harvested using a Nycodenz density gradient. pBCT was then electroporated into the purified schizonts, which were immediately injected into the tail veins of naïve mice. On the next day, the antimalarial drug, pyrimethamine (pyr) was administered in the drinking water of the mice to select for

transgenic parasites. I observed pyr-resistant transgenic parasites in the blood smears of mice eight to ten days post transfection. Once the infected mice reached a parasitemia of at least 10%, they were exsanguinated and the gDNA of the parasites was extracted for verification of *trxl-1* gene deletion.

Verification of Cas9-mediated Gene Deletion of *trxl-1*

For verification, I designed specific reporter primers as indicated in Figure 11 & 12. PCR analysis was carried out using the following DNA templates: wild type gDNA (WT), four samples of putative TrxL-1KO gDNA isolated from infected mice (KO1, KO2, KO3, KO4), and the plasmid pBCT. I also included a no template control (NTC).

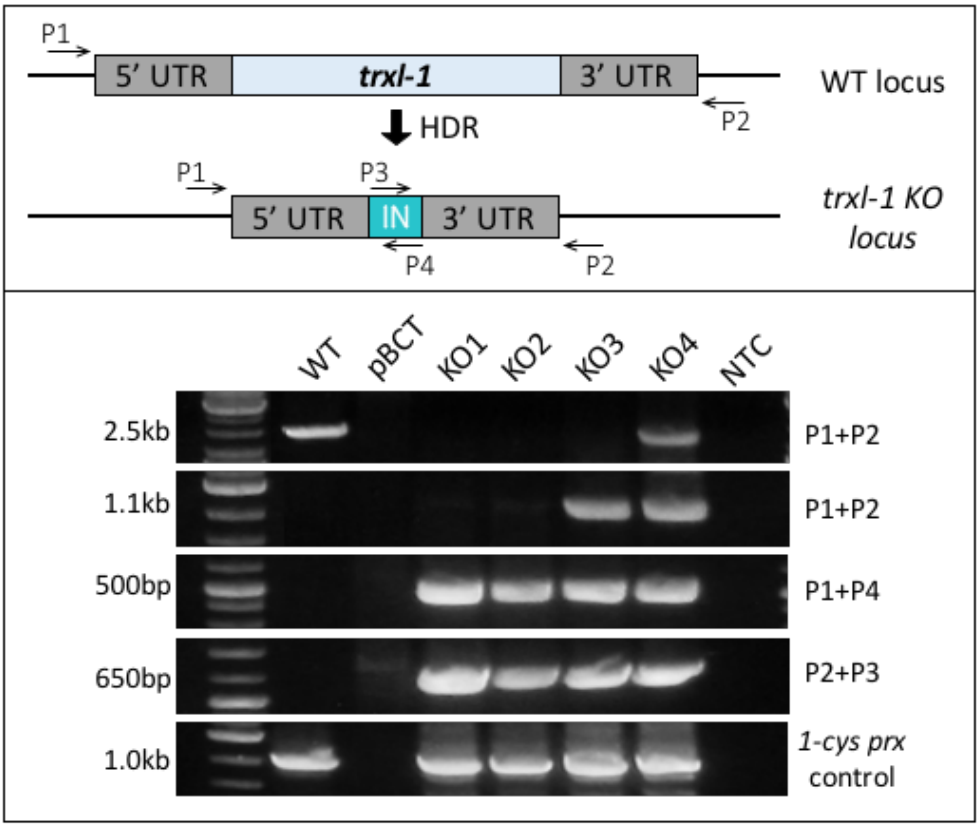

Figure 12 PCR Detection of *trxl-1* Gene Deletion. (TOP) Simplified schematic of WT and KO *trxl-1* locus and PCR primers used to detect gene deletion. (BOTTOM) DNA gel showing results of the PCR run with WT gDNA, a plasmid control (pBCT), four *trxl-1* KO gDNA samples (KO1-KO4) and a no template control (NTC).

To amplify the *trxl-1* locus, primers P1 and P2 were used (Figure 12). They are located outside of the *trxl-1* UTRs so that they recognized the gDNA template but not the homology construct on pBCT. The calculated amplicon size in the WT gDNA was 2.4 kb and the expected amplicon size for TrxL-1KO gDNA was calculated to be significantly shorter at 1.1 kb. The PCR results showed a clear band around 2.4 kb in the WT gDNA showing an unaltered *trxl-1* gene. In contrast, the KO4 gDNA sample showed a band around 1.1 kb indicating successful gene deletion of *trxl-1*. My KO1 and KO2 samples did not show any clear bands. The KO3 samples showed bands around 2.4 kb and 1.1 kb indicating a mixed population of WT and KO parasites. No amplification occurred in pBCT or NTC confirming that there was no cross-reactivity with the plasmid or contamination of my primers, respectively.

In addition, I checked for HDR-specific gene deletion (Figure 12). Primers P3 and P4 were designed to hybridize with the gene disrupter sequence (IN). The primer combinations, P1+P4 and P2+P3, can only amplify a product if the gene disrupter within the homology construct was integrated into the genome replacing the *trxl-1* gene. The expected amplicon size for P1+P4 was 500 bp and for P2+P3, it was 700 bp. For each of the TrxL-1KO gDNA samples, the PCR resulted in the expected bands for both of the primer sets. Concomitantly, these primer combinations did not produce bands in the WT gDNA, pBCT or NTC samples. Notably, the KO1 and KO2 samples contained the recombinant locus, even though there was no detectable amplification with the P1+P2 primer combination. The reason behind this is unclear.

To control for the integrity of all gDNA samples as well as the consistency of my preparation, I used primers specific to the *1-cys prx* gene (gDNA control), a single copy gene previously characterized in our lab (Turturice *et al.* 2013). The expected amplicon size was 1.0

kb. All PCR controls reactions resulted in the amplification of the expected 1.0 kb sized band in all gDNA samples while no amplification in pBCT or NTC sampes occurred (Figure 12).

The gDNA from the transgenic KO3 parasite population was the only sample producing the bands that correspond to the size of the *trxl-1* gene deletion, recombination via HDR, and no amplification of the WT locus. I therefore chose to generate clonal lines from the transgenic KO3 sample.

Generation of Clonal Parasite Lines

Parasite cloning is used to generate a population of genetically identical parasites. To this end, a sample of parasites from a mixed population will be serially diluted so that only a single parasite will be injected into the tail vein of a naïve mouse. I decided to use the KO3 population for parasite cloning since my PCR showed complete deletion of *trxl-1*. In my first attempt, I calculated for the injection of a single parasite directly into each of the tail veins of ten mice. After these attempts using one parasite per injection did not result in mouse infection, I increased the number to two parasites per injection. As a result, two out of ten of the mice that I injected showed blood stage parasites ten days post tail injection. These clones are herein referred to as clone 1 (c1) and clone 2 (c2).

I extracted the genomic DNA from each of the clonal lines for verification of gene deletion. After initial passage, clone 1 would not increase past 5% parasitemia. With such low infection rates, I could not verify gene deletion and continue with this clonal line. I have stored c1 at -80C for later analysis. Clone 2 was able to reach a higher parasitemia of around 35%, and I was able to verify gene deletion via PCR. For my thesis, I used c2, referred to as the TrxL-1KO line, for all subsequent phenotypic analyses.

Analysis of TrxL-1KO Parasites

I investigated the potential phenotype of the TrxL-1KO parasites utilizing the following methods. I first compared the growth rate of the TrxL-1KO clonal line to that of its parental WT strain during blood stage development. Second, I examined parasite development during the mosquito stages. I simultaneously assessed parasite morphology via light microscopy and immunofluorescence microscopy.

Trxl-1 is Not Essential in Blood Stage Development

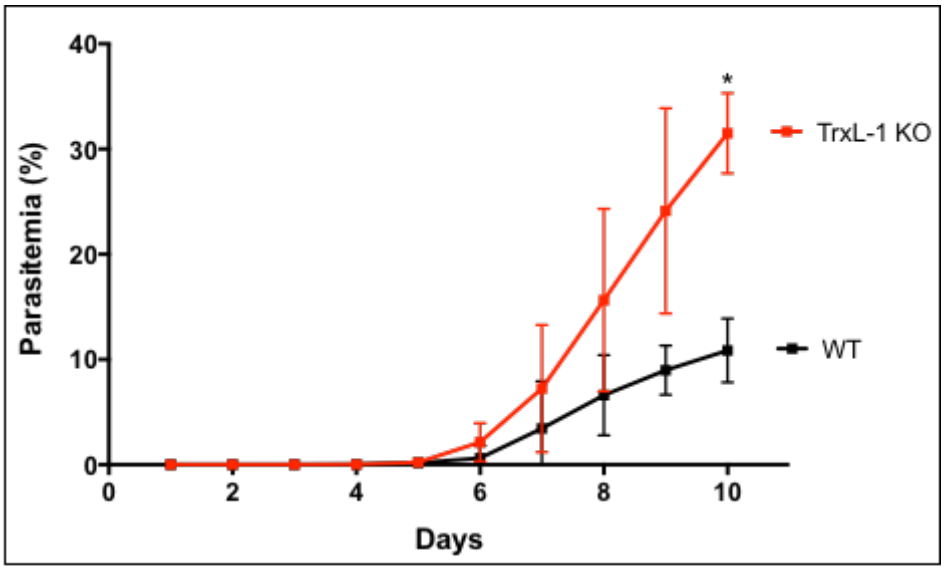

Figure 13 *Plasmodium berghei* Growth Curve in Blood Stages. Parasitemia measured over the course of 10 days post IV injection. Mean parasitemia taken from three independent experiments where N=16 (10 KO; 6 WT). Error bars represent STDEV. Statistical significance determined with GraphPad Prism software using multiple t-tests and the Holm-Sidak correction method. P *< 0.05.

To determine whether a phenotype was present in asexual stages, 2,000 parasites of WT and TrxL-1KO were each injected into the tail vein of a naïve mouse. For each experiment, I injected three mice with WT and three mice with TrxL-1KO parasites. The parasitemia was measured daily by counting the number of infected red blood cells.

The data was compiled and the mean parasitemia over time was plotted for the WT and TrxL-1KO (Figure 13).

The growth curve indicated that both TrxL-1KO and WT parasites were visible in the blood smears by day five. The mice infected with WT began to show symptoms such as ruffled fur, lethargy, pale eyes, and respiratory distress, around day eight or day nine with parasitemia ranging from 10-15%. In contrast, the TrxL-1KO parasites seemed to show much more variability in growth rate and parasitemia. They reached as high as 35 – 40% parasitemia without showing any symptoms. These results clearly indicate that TrxL-1 is not essential in blood stage development. However, the variability in TrxL-1KO parasitemia made phenotypic analysis difficult as the data does not conclusively show that the TrxL-1KO parasites grow at a significantly different growth rate than WT parasites.

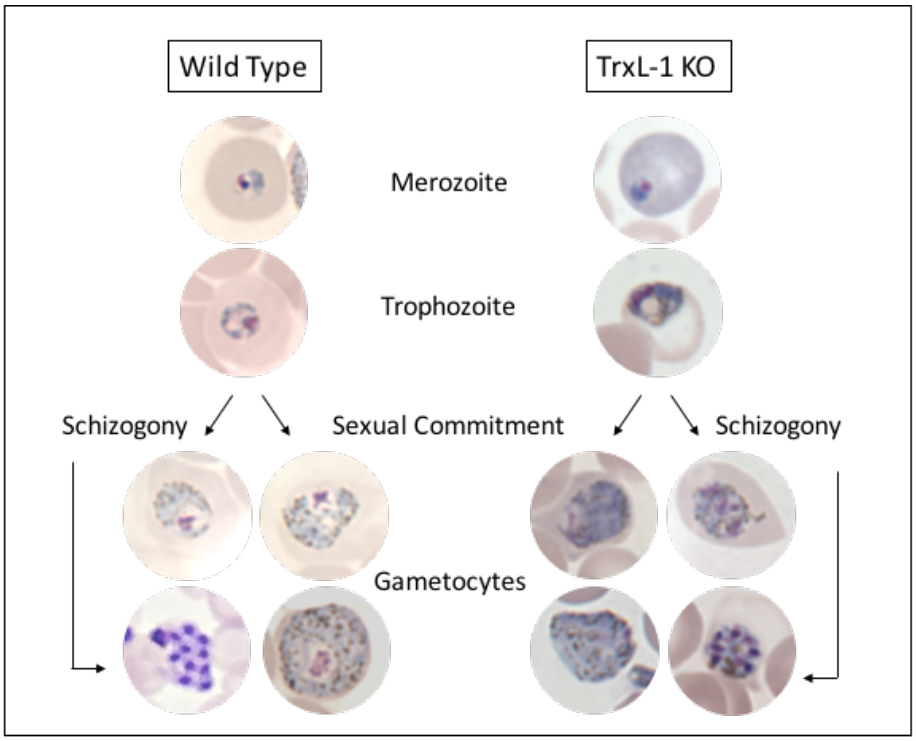

Figure 14 Blood Stage Parasite Morphology. A side by side comparison of wild type and TrxL-1KO blood stage parasites. All parasites were stained with Giemsa and viewed at 1000X magnification.

Trxl-1 Does Not Affect Morphology in Blood Stages

Because TrxL-1 could be potentially affecting the shape of the parasite, I examined parasite morphology during the blood stages. I did not find any discernable differences between the WT and TrxL-1KO parasites in any of the blood stages including merozoites, trophozoites, schizonts, and gametocytes. A comparison of the WT and TrxL1-KO parasites is shown in Figure 14.

Trxl-1 is Involved in Mosquito Stage Development

Next, I expanded my investigation of the potential phenotype to the mosquito stages of development. Specifically, I examined the maturation of ookinetes within the mosquito midgut over the course of 24 hours. To better describe the development of the ookinetes, I used previously establishing maturation stages (Sinden *et al.* 2004) (Figure 15).

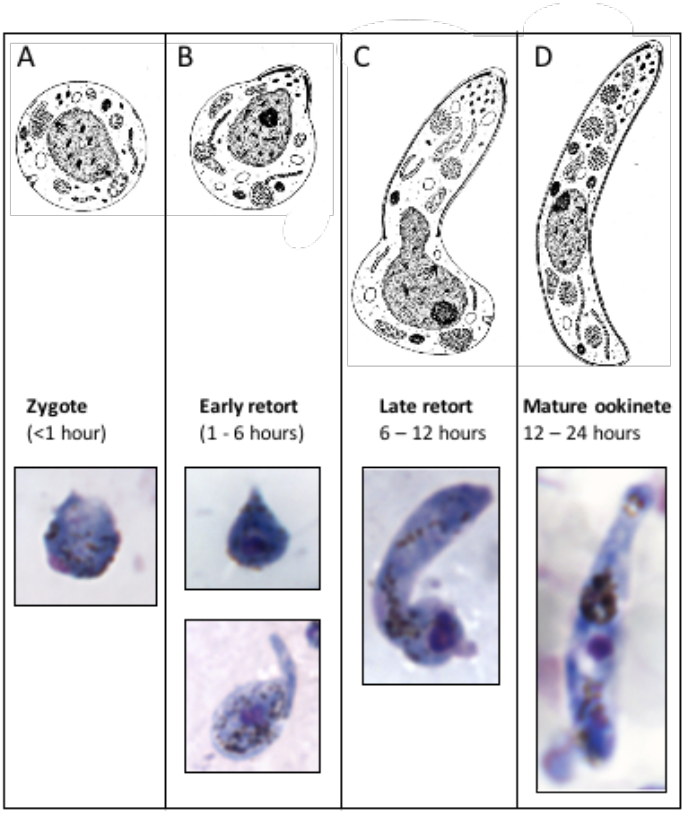

Figure 15 *Plasmodium* ookinete development.
Top panel (A-D) Diagrams illustrating *Plasmodium* ookinete development (taken from: Sinden et al. Ookinete Cell Biology. Chapter 15 of Malaria Parasites: Genomes and Molecular Biology Caister Academic Press, 2004). Time periods refer to hours post ookinete culture setup.
Bottom panel: Developing *P. berghei* ookinetes from our lab, methanol-fixed and giemsa stained.

Five to eight day old mosquitoes were allowed to feed on WT or TrxL-1KO infected mice for 15 minutes. 12, 18, and 24 hours post infectious blood meal (PIBM), I dissected and smeared five bloodfed mosquito midguts from each cohort. I selected 12 hours PIBM as my first time point because the maturity level prior to this point could not be determined via light microscopy. Data was collected from three independent feeds with independent cohorts of mosquitoes and mice. The relative number of mature ookinetes was quantified for each dissected mosquito midgut at each time point. The percentage of mature TrxL-1KO ookinetes was compared with the percentage of mature WT ookinetes (Figure 16).

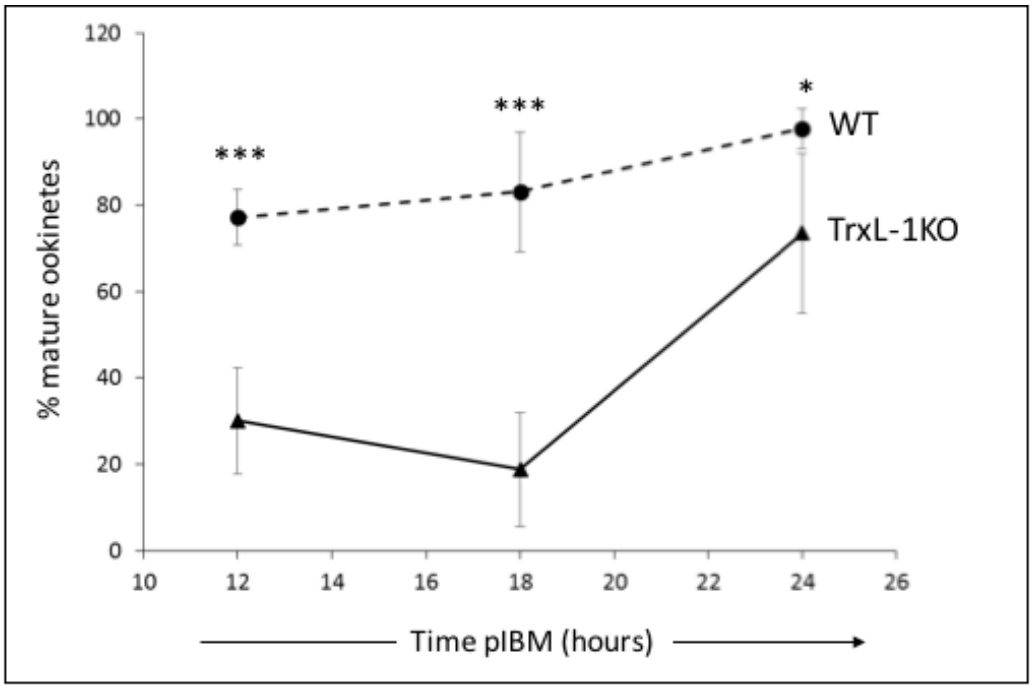

Figure 16 Ookinete Development of WT and TrxL-1KO parasites in the Mosquito. Mosquitoes were fed on Wild Type (WT) and TrxL-1 KO infected mice. Midguts were dissected at 12, 18, and 24 hours post feed (3 individual feeds, 5 midguts per time point). Error bars represent ±STDEV. Statistical significance of difference in mature ookinete numbers was determined using an independent *t* test. *P<0.05 ***P<0.001.

Compared to WT ookinetes, the data shows a significant reduction in the number of mature TrxL-1KO ookinetes. I found that 12 hours PIBM, 76% of the wild type (WT) ookinetes were fully developed, while only 30% of the TrxL-1KO ookinetes were mature. At 18 hours

PIBM, 80% of WT ookinetes being mature, in comparison to 20% of the TrxL-1KO ookinetes being fully developed. By 24 hours, almost 100% of WT ookinetes were found to be mature while only 65% of TrxL-1 ookinetes were mature. The growth delay seen in the TrxL-1KO ookinetes indicates that *trxl-1* does play a role in the mosquito stage development.

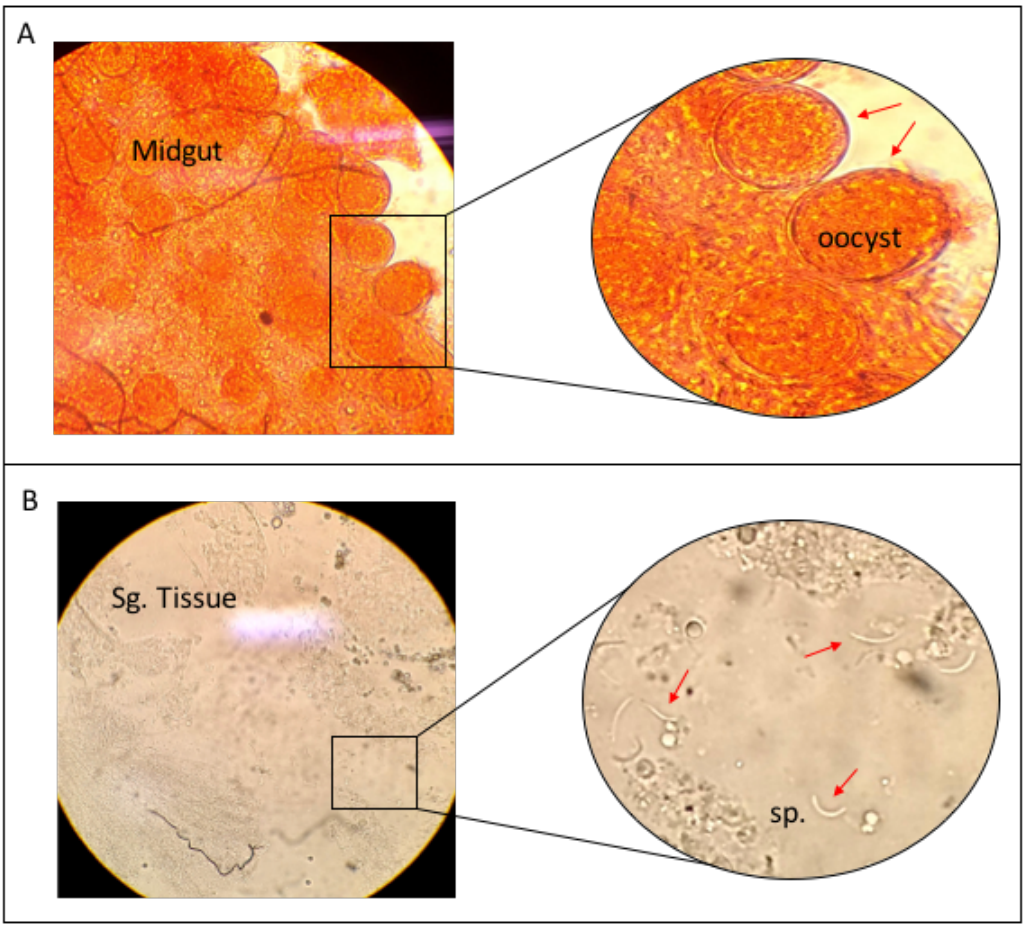

Figure 17 Oocyst and Sporozoite Development. (A) Mercurochrome staining of a dissected TrxL-1KO bloodfed midgut embedded with TrxL-1KO oocysts (red arrows). (B) Burst salivary gland (Sg.) taken from TrxL-1KO bloodfed mosquito with sporozoites (sp.) moving out of the tissue (red arrows indicate single sporozoites).

To determine whether the TrxL-1KO ookinetes could continue to develop in the mosquito (see Figure 1), I dissected midguts on day 9 and day 15 to examine oocyst formation and removed salivary glands on day 21 to detect sporozoite formation. To visualize the oocysts, I stained the dissected midguts with mercurochrome and viewed them under 400X magnification.

I found that TrxL-1KO ookinetes were able to traverse the midgut lining and develop into oocysts (Figure 17A). To visualize the sporozoites, the salivary glands were dissected, crushed under the pressure of a coverslip, and viewed under 400X magnification. I found that the TrxL1-KO parasites successfully developed into sporozoites as I was able to observe them flowing out of the salivary glands (Figure 17B).

Once TrxL-1KO salivary gland sporozoites were confirmed, the infected mosquitoes were allowed to feed on naïve mice to determine whether the TrxL-1KO parasites could infect the mice and complete the life cycle. Twelve days post infectious feed, I found blood stage parasites in the mice, confirming that the TrxL-1KO sporozoites were infectious to hepatocytes and completed the life cycle.

TrxL-1 Specifically Affects Ookinete Development and Morphology

Because I hypothesized that TrxL-1 is involved in maintaining the shape of the parasite, I next examined the morphology of the ookinetes under light microscopy and immunofluorescence microscopy.

For light microscopy, ookinetes were smeared on slides and processed as previously described in the materials and methods. In the smears, I found that many TrxL-1KO ookinetes from both the midguts and cultures possessed distinct morphological deformities (Figure 18). Compared to the midgut WT ookinetes (Figure 18A), some of the TrxL-1KO ookinetes were not able to maintain their characteristic banana-shape while others could not elongate at all (Figure 18B). In the cultures, I also found that many TrxL-1KO ookinetes appeared to be either deflated with particularly thin portions of the membrane or overinflated with large, bulbous protrusions (Figure 18D).

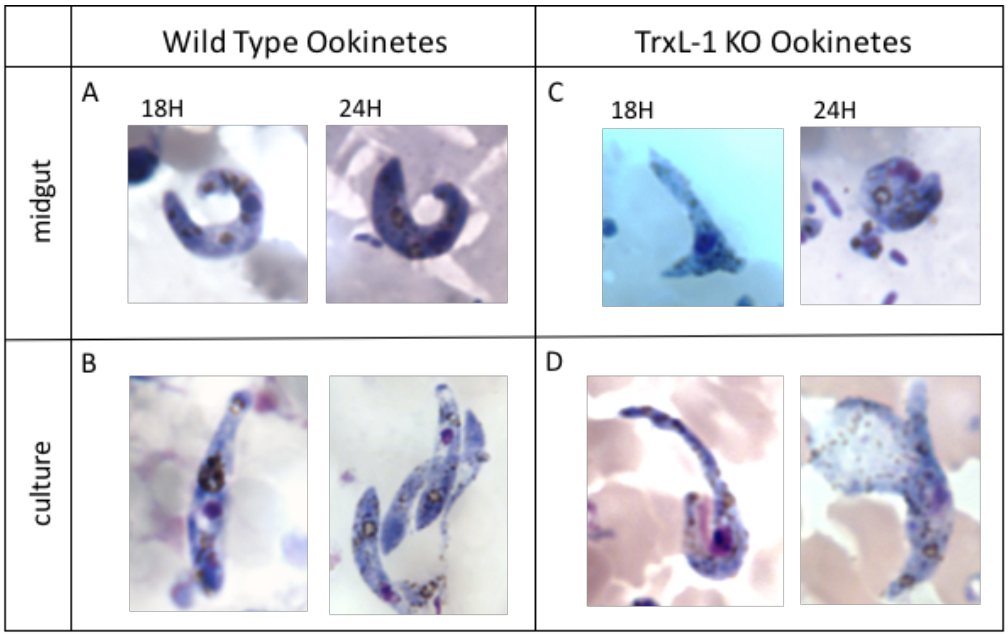

Figure 18 Morphological Deformities of TrxL-1 KO Ookinetes. (A) Wild type ookinetes in the mosquito midgut 18 and 24 hours PIBM. **(B)** Wild type ookinetes in culture 18 and 24 hours post culture setup. **(C)** TrxL-1 KO ookinetes in the mosquito midgut 18 and 24 hours PIBM. **(D)** TrxL-1 KO ookinetes in culture 18 and 24 post culture setup. All ookinetes stained with Giemsa.

To determine if these morphological deformities are due to the destabilization of microtubules, I used immunofluorescence to visualize the organization of microtubules in the ookinetes. To this end, I set up mosquito feeds and ookinete cultures with WT and TrxL-1KO parasites and prepared them for immunofluorescence labeling as detailed in the methods and materials. I co-labeled the parasites with anti-PbTrx-1 antibodies and anti-α-tubulin antibodies graciously provided by Dr. Jennifer Mierisch. The tubulin antibodies localize specifically to the periphery of the cell as they label the microtubules. Our lab has previously shown that thioredoxin-1 (Trx-1) is a ubiquitously expressed protein in the cytosol of all *P. berghei* stages (Turturice et al. 2013). I therefore used anti-PbTrx-1 antibodies to mark Thioredoxin-1 as a cytosolic control. Parasites were imaged using confocal microscopy. To image the surface and

middle sections of the ookinete, separate slices of the parasites were captured via scanning through the sample.

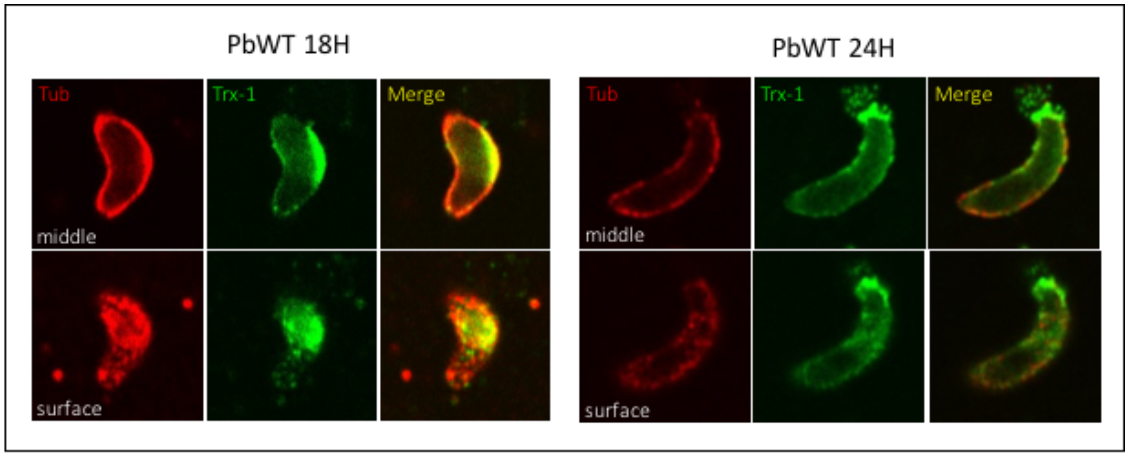

Figure 19 Immunofluorescence Staining of WT Ookinetes. Immunoflourescence staining with WT midgut ookinetes 18 hours and 24 hours PIBM. Co-staining with anti-tubulin antibodies (red) and anti-thioredoxin-1 antibodies (green). The middle cross-section of the ookinete and surface of the ookinete are shown.

The WT ookinetes showed distinct staining of tubulin localizing to the periphery of the cell while Trx-1 was observed throughout the whole cell (Figure 19). The TrxL-1KO ookinetes also displayed anti-PbTrx-1 staining throughout the entire length of the ookinete. However, unlike the WT ookinetes, the TrxL-1KO ookinetes did not show distinct staining of tubulin on the periphery (Figure 20).

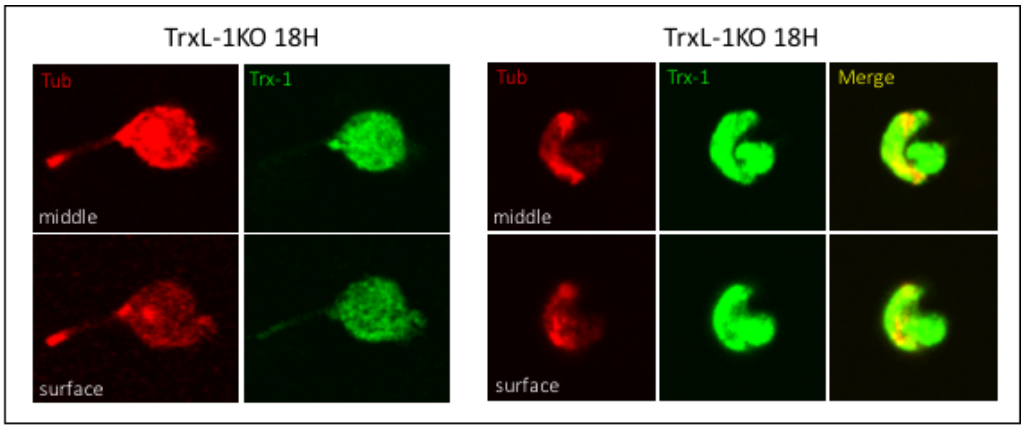

Figure 20 Immunofluorescence Staining of TrxL-1KO Ookinetes. IFA with TrxL-1KO cultured ookinetes 18 hours post culture set up. Co-staining with anti-tubulin antibodies (red) and anti-thioredoxin-1 antibodies (green). The middle cross-section of the ookinete and surface of the ookinete are shown.

In the middle and surface cross sections, tubulin was also stained throughout the whole cell. Interestingly, the strong staining throughout the middle section suggested that most of the tubulin in the ookinete was cytosolic. I did not find any stained ookinetes from the TrxL-1KO midguts or 24-hour culture slides. Although more imaging is required, there is a strong indication that the stability of the microtubules is affected by the loss of TrxL-1.

Disruption of *spm-1* in *P. berghei*

In parallel with the phenotypic analysis of the TrxL-1KO parasites, I was also working on the construct to delete the *spm-1* gene (Figure 21). I generated a *spm-1* specific TS using Geneious as previously described for *trxl-1*. Because of the previous cloning problems with the small 20 bp TS oligonucleotide, I instead engineered the *spm-1* TS into primers so that it will be integrated directly into the sgRNA scaffold on pBC. I used pBC as the DNA template and cloned the resulting TS-sgRNA amplicon into pGEM. I then cloned the *spm-1* TS-sgRNA into pBC.

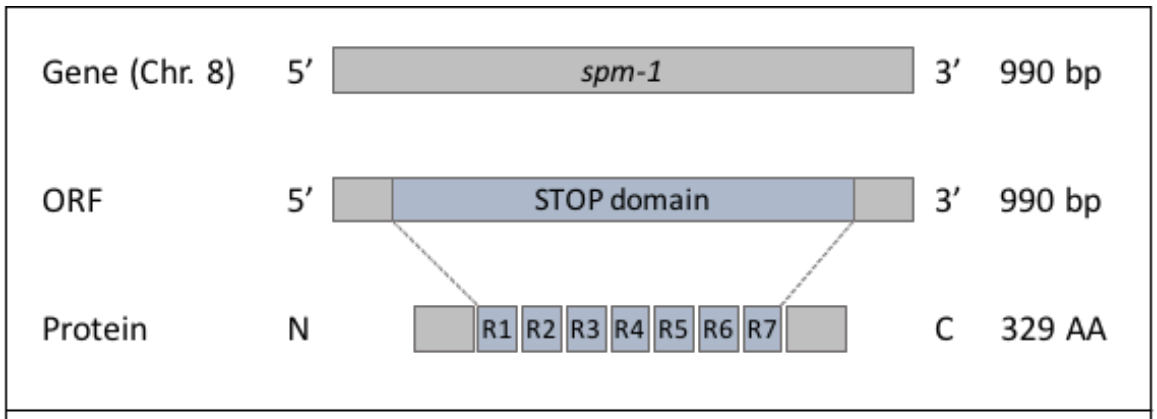

Figure 21 Organization of PbSPM-1. Representation of the gene, the putative open reading frame (ORF), and the primary structure. SPM-1 contains a STOP domain indicated in blue. This domain contains seven repeats (R1-R7).

To generate the homology construct, I used PCR to amplify the 5' HA and 3' HA of *spm-1*. I then cloned the two homology arms into a separate vector as previously described for *trxl-1*. I named the resulting SPM-1KO plasmid pBCS for plasmid for *P. berghei* CRISPR/Cas9

mediated SPM-1KO (Figure 22). pBCS was transfected into PbWT schizonts and injected into naïve mice. Transgenic parasites were selected for using pyr. Drug resistant parasites were detected in the blood eight days post injection. The genomic DNA was extracted from five separate transgenic parasite populations.

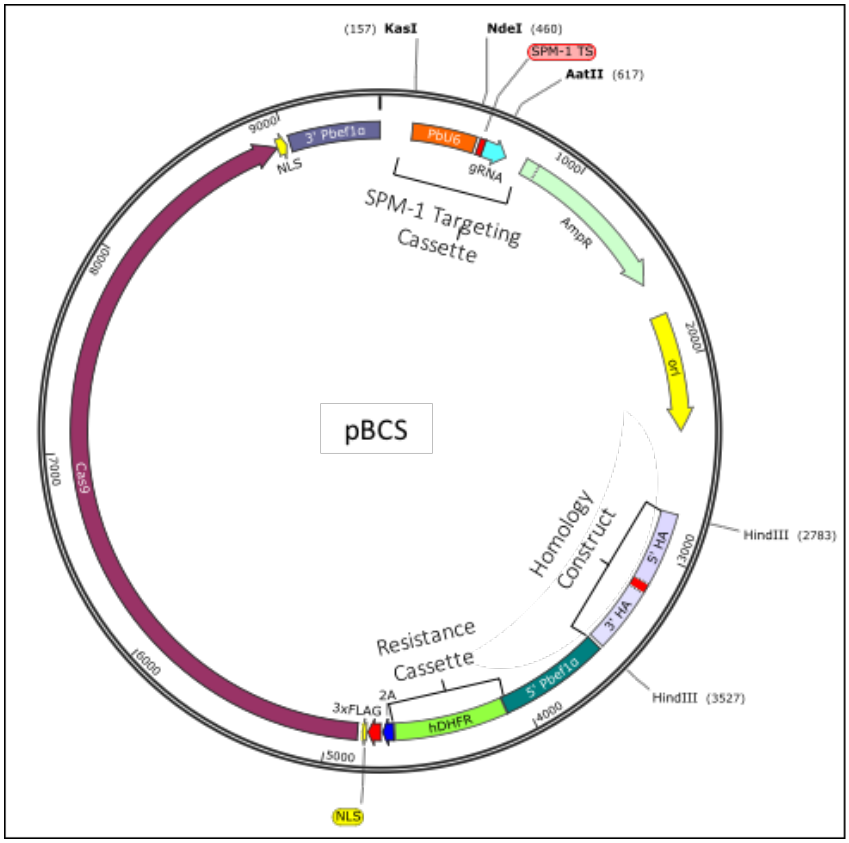

Figure 22 Plasmid Map of pBCS. Generated plasmid map showing all of the necessary elements of the SPM-1 KO plasmid, pBCS. It contains a *P. berghei* U6 promoter (PbU6) driving expression of the *trxl-1* target sequence (SPM-1 TS) and the guide RNA (gRNA), a *P. berghei* promoter (Pbef1α) driving the expression of the pyrimethamine resistance gene (hDHFR) and the 2A FLAG-Cas9 gene, a *spm-1* homology construct with both 5' and 3' homology arms (HA), and an ampicillin resistance gene (AmpR). Map generated with SnapGene software (GSL Biotech).

Verification of Cas9-mediated Gene Deletion of *spm-1*

To detect successful *spm-1* deletion, initial PCR analysis was conducted using primers specific to the 5' HA and 3' HA of *spm-1* (Figure 23). The DNA templates used were: WT gDNA, five SPM-1KO (KO1-KO5) gDNA samples, pBCS, and a no template control (NTC). As expected, the WT gDNA generated an amplicon around 2.0 kb. Other than primer dimers, no amplification was observed in the NTC. Because pBCS contains the homology construct for *spm-1*, pBCS was used as a control to detect the expected amplicon size of the *spm-1* deletion.

Three of the SPM-1KO samples (KO1, KO2, and KO5) resulted in no amplification. Two KO samples (KO3 and KO4) resulted in the amplification of the gDNA samples. KO3 showed a band around 2.0 kb which indicates that there was no gene deletion in that sample. Only one of the samples (KO4) contained a 1.0 kb band which indicates successful gene knockout. The KO4 sample also showed two additional bands around 1.5 and 2.0 kb indicating a mixed population. Because KO4 showed gene deletion, this population was selected for cloning in order to generate a SPM-1KO clonal line. Once cloned, additional primers for the gene disrupter and outside of the 5' and 3' HA on pBCS must be used in order to verify complete *spm-1* knockout.

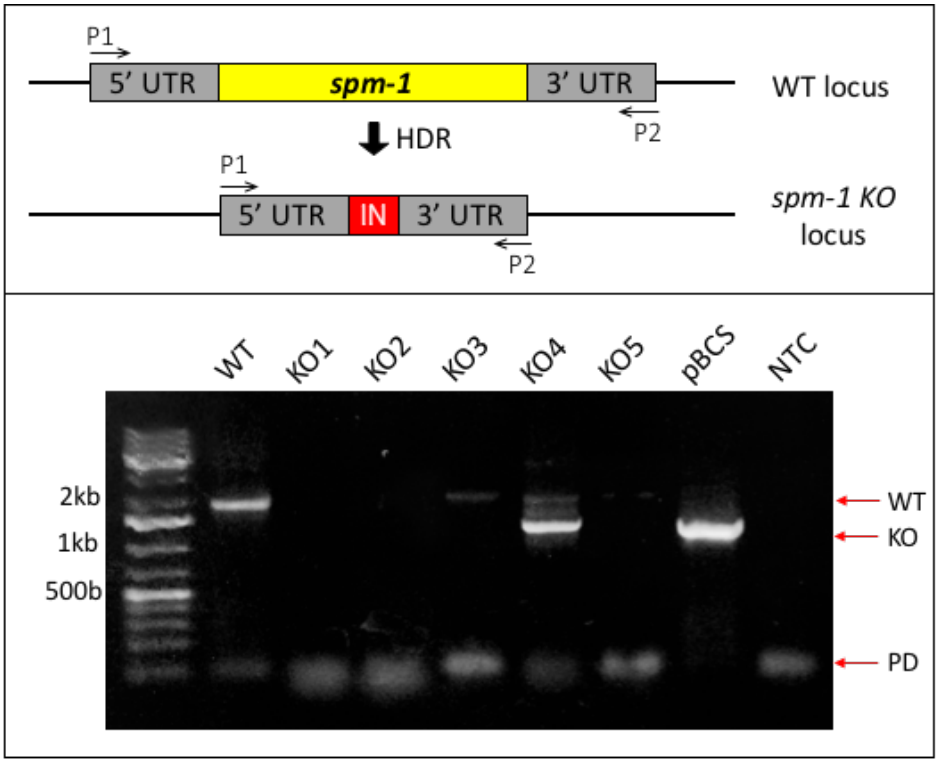

Figure 23 Initial PCR Detection of *spm-1* Gene Deletion. PCR primers (P1 and P2) were used to detect the deletion of *spm-1*. DNA templates used were WT gDNA, five *spm-1* KO gDNA samples (KO1-KO5), pBCS, and a no template control (NTC). Red arrows indicate the bands corresponding to the expected WT amplicon, KO amplicon, and the presence of primer dimers (PD).

Initial Analysis of SPM-1KO Parasites in Blood Stages

Once I confirmed the deletion of *spm-1*, I examined the parasites in the blood stages of development. Similar to the TrxL-1KO, I found that the SPM-1KO parasites were able to successfully infect the mice. The SPM-1KO infected mice reached parasitemias as high as 60% and did not show any symptoms. These results show that *spm-1* is not essential for blood stage development. In contrast to the TrxL-1KO parasites, I found that there are morphological deformities in the SPM-1KO schizonts (Figure 24). In comparison to the WT schizonts that contain eight to twelve merozoites per cell (Figure 24 A), a portion of the SPM-1KO schizonts only contain four to eight merozoites (Figure 24 B). Additionally, the merozoites within each of the SPM-1KO schizonts appear to be more scattered and less organized than in the WT schizonts.

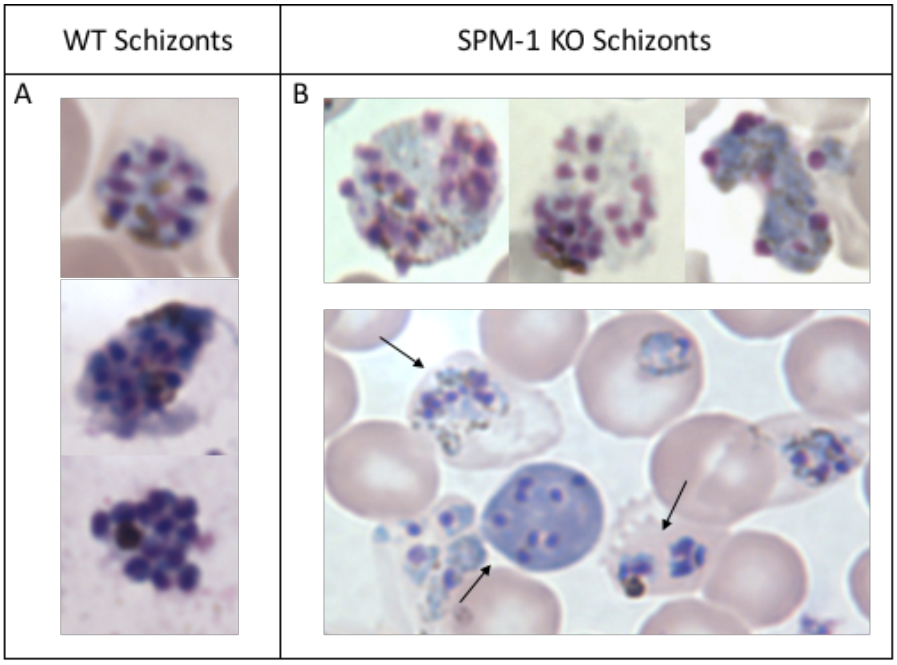

Figure 24 Morphological deformities in SPM-1 KO Schizonts. A side by side comparison of WT (A) and SPM-1KO (B) schizonts during blood stage development. Arrows indicate the misformed schizonts in the bottom image. All schizonts stained with Giemsa and viewed at 1000X magnification.

CHAPTER IV

DISCUSSION

The purpose of this thesis was to establish the CRISPR/Cas9 gene editing system in *P. berghei* and use it to investigate the function of two novel *Plasmodium* genes, *trxl-1* and *spm-1*. Genetic manipulation of *Plasmodium* remains a challenge as most methods are time consuming, inefficient, and expensive (Straimer *et al.* 2012; Wu *et al.* 1996). The CRISPR/Cas9 system represents an opportunity to reduce the cost and increase efficiency of genomic editing in the prominent mouse model parasite *P. berghei*.

In this study, I established the CRISPR/Cas9 system in *P. berghei* and successfully edited the genome resulting in the generation of two gene KO parasite lines, TrxL-1KO and SPM-1KO. I found that *trxl-1* is not an essential gene and is involved in ookinete development within the mosquito midgut. Additionally, I found that the loss of *spm-1* is not lethal in asexual stages, but appears to be important for schizogony and gametocytogenesis in the malaria parasite.

The establishment of the CRISPR/Cas9 system increases our ability to manipulate the *P. berghei* genome and subsequently advances the rate at which we can conduct functional studies. As gene deletion is often the first approach to investigating gene function, I used CRISPR/Cas9 to knockout my genes of interest. Traditional gene knockout methods rely on the transfection of a plasmid, containing a drug resistance cassette, and simple homologous recombination with the genome to replace a targeted gene (Wu *et al.* 1996). This technique requires months of drug selection and cloning following transfection of the plasmid with highly variable success.

In contrast, with the help of the CRISPR/Cas9 system, I generated KO parasite lines within just two weeks following transfection of the KO plasmids. Moreover, the resulting KO parasite lines did not require months of constant drug pressure because CRISPR/Cas9 produces a stable, targeted deletion and a quick, effective integration of the gene disrupter sequence. In comparison to other studies that used CRISPR/Cas9, such as the editing of the *P. falciparum* genome that required co-transfection of two plasmids (Wagner *et al.* 2014), I generated each parasite line with the transfection of one plasmid. Using a single plasmid greatly increased the efficiency of the generation of transgenic parasites, which subsequently improved the chance of successful Cas9-mediated gene KO.

The first gene I knocked out was *trxl-1.* As the TrxL-1KO parasites successfully infected and reproduced within the mouse blood and mosquito stages, I determined that *trxl-1* is not an essential gene. In the blood stages, I did not detect any TrxL-1KO growth phenotype, and there were no observable differences in TrxL-1KO parasite morphology when compared to WT parasites. These findings are comparable to the data from *T. gondii* as the researchers also did not detect a growth phenotype in the TgTrxL-1 knockout parasites (Liu *et al.,* 2013). Interestingly, I found that although *trxl-1* is dispensable for *P. berghei*, the knockout parasites seem to become less virulent as infected mice tolerated a much higher parasitemia, at times up to 45%.

Additionally, many of the infected mice did not show any signs of illness that would be expected at such high parasitemia. The functional significance of this loss of virulence remains unknown and would be an interesting area to pursue in the future. One possible explanation is that the TrxL-1KO parasites do not illicit an immune response that is as strong as it is during WT *P. berghei* infection. To test for this, we can begin by checking the TrxL-1KO blood smears for activated white blood cells.

Supporting my hypothesis that *trxl-1* is involved in mosquito stage development, I found that the growth of TrxL-1KO ookinetes is significantly delayed when compared to the WT ookinetes. At 18 hours PIBM, I found that approximately 80% of TrxL-1KO ookinetes were immature. I also observed distinct morphological deformities in the TrxL-1KO ookinetes when compared to WT. The normal banana-like shape of the ookinetes is not retained and in some cases, not established at all. As the subpellicular microtubules are known to support the parasite's shape (Baum *et al.*2006) and the *T. gondii trxl-1* homolog showed an interaction with microtubules, *trxl-1* could be playing a role in the stabilization of the microtubules in the development of *Plasmodium* ookinetes.

A subset of TrxL-1KO ookinetes were capable of maturing into their proper shape and successfully infecting the mosquito. One explanation is that there could be a compensatory mechanism allowing these ookinetes to function normally. In *T. gondii,* it was found that the TgTrxL-1 protein is part of a microtubule associated protein complex that consists of the subpellicular microtubule protein 1 (TgSPM-1), thioredoxin-like protein 2 (TgTrxL-2), and other novel TrxL1-associating proteins, TgTLAP-1 and TgTLAP-2 (Liu *et al.,* 2013). However, a screen of the *P. berghei* genome revealed that *Plasmodium* lacks a *trxl-2* homolog. Homologs for SPM-1, TLAP-1, and TLAP-2 are present in the rodent parasite and it is possible that they have the capacity to compensate for the loss of *trxl-1*. On the other hand, since *T. gondii* does not require an insect vector, the conditions that control microtubule stability and regulation may be different. Because *Plasmodium* parasites are exposed to the harsh conditions of the mosquito midgut, I would expect the proteins lining and controlling regulation of the subpellicular microtubules to play a more important role in the malaria parasite than in *Toxoplasma*.

A closer inspection of the *Plasmodium* microtubules via immunofluorescence revealed that the microtubules in the TrxL-1KO ookinetes appear to be less organized and are not clearly localized to the periphery of the cell (Figure 25). This could compromise the overall banana-shape of the maturing ookinete.

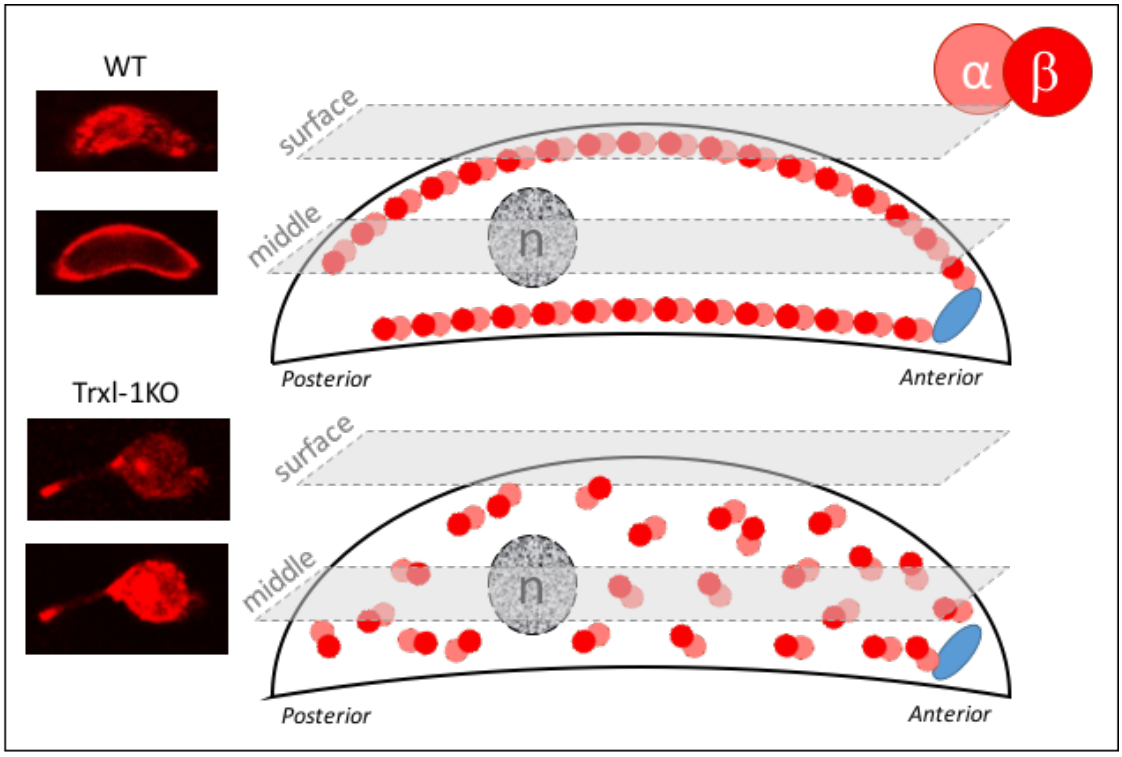

Figure 25 Representation of Microtubule Organization of WT and TrxL-1KO Ookinetes. (LEFT) Images of WT and TrxL-1KO ookinetes labeled with anti-tubulin antibodies. (RIGHT) Representation of the organization of α-tubulin/β-tubulin dimers in the WT and TrxL-1KO ookinetes where the surface and middle cross sections are indicated and 'n' indicates the nucleus of the ookinete.

This suggests that the loss of *trxl-1* prevents the localization of microtubules to the periphery of the cell and consequently negatively affects ookinete elongation, shape formation, and rate of development. While this data serves to initially characterize the molecular function of TrxL-1, further investigation is necessary in order to confirm the effect on microtubule stabilization and parasite biology. On top of additional immunofluorescence microscopy, viewing the parasites under a higher resolution, such as electron microscopy, would provide a

much more detailed look into the morphology and underlying cytoskeletal organization. Another approach that we could use to confirm these findings is a *trxl-1* gene rescue by providing the parasites with a plasmid containing the functional *trxl-1* gene. If normal ookinete development and morphology is restored, we would confirm that the phenotype we have observed is due to the loss of *trxl-1*.

In *Toxoplasma*, the TrxL-1 protein was shown to indirectly associate with the subpellicular microtubules via an interaction with SPM-1 (Liu *et al.,* 2013), which is why I decided to knockout *spm-1* in *P. berghei.* Similar to *trxl-1*, I found that *spm-1* is not essential for the development of the asexual blood stages in the mouse. However, my preliminary analysis of the SPM-1KO parasites showed that the SPM1-KO schizonts appear to have morphological differences when compared to WT. For example, no distinct equally sized merozoites can be identified and the number of merozoites is very low when compared to WT parasites. Furthermore, very few mature gametocytes have been identified in the blood smears of the SPM-1KO infected mice. These initial observations are currently being verified and quantified in our lab.

Interestingly, if *spm-1* is confirmed to be involved in schizogony or gametocytogenesis, the overall effects of the SPM-1KO may be more detrimental than the TrxL-1KO. During schizogony, the pellicle of the merozoites is supported by the underlying subpellicular microtubules. Because *spm-1* may potentially play a role in the stabilization of these subpellicular microtubules, pellicle formation may be negatively affected by the loss of *spm-1*. On the other hand, if gametocytogenesis is negatively affected, I would expect a more severe phenotype in early mosquito stages. Microtubule associated proteins, such as the STOP Axonemal protein (SAXO-1) in the flagellated, protozoan parasite *Trypanosoma brucei*

(Dacheux *et al.*, 2012), have been shown to stabilize microtubules by conferring cold-resistance. This study also demonstrated that TbSAXO-1 is involved in flagellum motility. As *Plasmodium* experiences a temperature drop in the mosquito vector and requires the production of exflagellating gametocytes, *spm-1* may be functioning in a similar way to TbSAXO-1. Without the exflagellation of gametocytes, there would be no fertilization and thus no ookinetes. If the ookinetes cannot develop, the life cycle ends in the mosquito, effectively blocking transmission to the next host. As additional analyses are required to characterize this phenotype, members of my lab are eagerly continuing to investigate the role of *spm-1* in all stages of parasite development.

Beyond discovering the cellular function of *trxl-1* and *spm*-1, this thesis sheds light on the regulation of the subpellicular microtubules. In recent years, the thioredoxin system has been implicated in the redox regulation of important cellular pathways and structures. Certain changes in the redox potential of the cell, such as the production of ROS, can influence the state of cellular structures, including microtubules and flagella (Aksenova *et al.*, 2001; Wakabayashi and King, 2006).

Biochemical characterization of both TrxL-1 and SPM-1 proteins in our lab revealed that they are redox active and that each is efficiently reduced by the thioredoxin system. An intriguing possibility is that the association of TrxL-1 with its target proteins, such as SPM-1, may be redox based. In light of these findings, it is possible that in *Plasmodium,* TrxL-1 and/or SPM-1 represent a direct link between the cellular redox regulatory system and the cytoskeleton, in this case the microtubules. I have included a hypothetical model representing the connection

between the Trx-mediated redox homeostasis of the cell and microtubule stability via the interactions between TrxL-1 and SPM-1 (Figure 26).

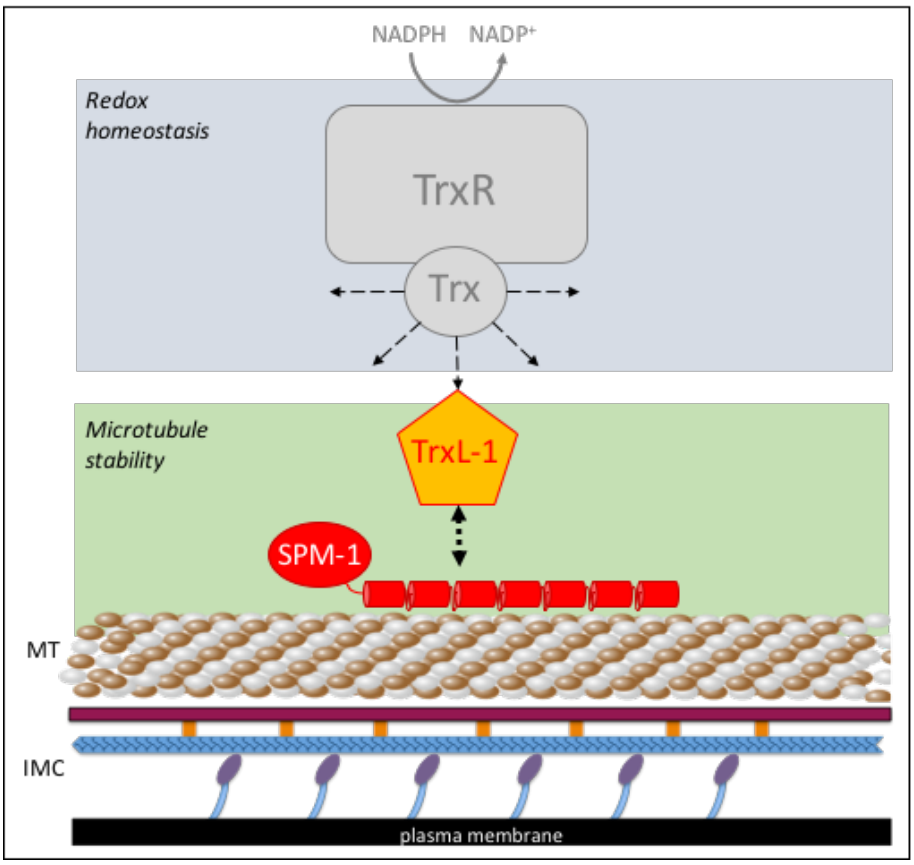

Figure 26. Model of the Protein Complex with the Subpellicular Network. Representative model of the potential SPM-1 and TrxL-1 protein complex associated with the subpellicular network of *Plasmodium*. The top represents the potential regulation within the thioredoxin (Trx) system and the bottom indicates the involvement with the subpellicular microtubule (MT) network of the inner membrane complex (IMC).

With this study, I am the first to establish the CRISPR/Cas9 system in *P. berghei.* I successfully adapted this system to modify the *P. berghei* genome and generated two gene KO parasite lines with high efficiency (100% gene deletion for each *trxl-1* and *spm-1*.) The functional characterization of TrxL-1 revealed that it plays a role in parasite development in the mosquito vector, specifically in the generation and maintenance of the banana-like ookinete shape. We have shown that TrxL-1 is potentially regulated by the Trx system and is involved in the stabilization of the subpellicular microtubules via SPM-1. Overall, this study contributes to

our fundamental understanding of the regulation of microtubules and reveals a potential mechanism for parasite development and survival in the mosquito vector.

REFERENCE LIST

Achard, M.E.S., Hamilton, A.J., Dankowski, T., Heras, B., Schembri, M.S., Edwards, J.L., Jennings, M.P., and McEwan, A.G. (2009). A Periplasmic Thioredoxin-Like Protein Plays a Role in Defense against Oxidative Stress in Neisseria gonorrhoeae. Infect. Immun. *77*, 4934–4939.

Aksenov, M.Y., Aksenova, M.V., Butterfield, D.A., Geddes, J.W., and Markesbery, W.R. (2001). Protein oxidation in the brain in Alzheimer's disease. Neuroscience *103*, 373–383.

Alavi, Y., Arai, M., Mendoza, J., Tufet-Bayona, M., Sinha, R., Fowler, K., Billker, O., Franke-Fayard, B., Janse, C.J., Waters, A., et al. (2003). The dynamics of interactions between Plasmodium and the mosquito: a study of the infectivity of Plasmodium berghei and Plasmodium gallinaceum, and their transmission by Anopheles stephensi, Anopheles gambiae and Aedes aegypti. International Journal for Parasitology *33*, 933–943.

Altschul, S.F., Gish, W., Miller, W., Myers, E.W., and Lipman, D.J. (1990). Basic local alignment search tool. Journal of Molecular Biology *215*, 403–410.

Arnér, E.S.J., and Holmgren, A. (2000). Physiological functions of thioredoxin and thioredoxin reductase. European Journal of Biochemistry *267*, 6102–6109.

Ashley, E.A., Dhorda, M., Fairhurst, R.M., Amaratunga, C., Lim, P., Suon, S., Sreng, S., Anderson, J.M., Mao, S., Sam, B., et al. (2014). Spread of Artemisinin Resistance in Plasmodium falciparum Malaria. New England Journal of Medicine *371*, 411–423.

Aurrecoechea, C., Brestelli, J., Brunk, B.P., Dommer, J., Fischer, S., Gajria, B., Gao, X., Gingle, A., Grant, G., Harb, O.S., et al. (2009). PlasmoDB: a functional genomic database for malaria parasites. Nucleic Acids Res *37*, D539–D543.

Bargieri, D., Lagal, V., Andenmatten, N., Tardieux, I., Meissner, M., and Ménard, R. (2014). Host Cell Invasion by Apicomplexan Parasites: The Junction Conundrum. PLoS Pathog *10*.

Baum, J., Papenfuss, A.T., Baum, B., Speed, T.P., and Cowman, A.F. (2006). Regulation of apicomplexan actin-based motility. Nat Rev Micro *4*, 621–628.

Baum, J., Gilberger, T.-W., Frischknecht, F., and Meissner, M. (2008). Host-cell invasion by malaria parasites: insights from Plasmodium and Toxoplasma. Trends in

Parasitology *24*, 557–563.

Black, M.W., and Boothroyd, J.C. (2000). Lytic Cycle of Toxoplasma gondii. Microbiol Mol Biol Rev *64*, 607–623.

Cong, L., Ran, F.A., Cox, D., Lin, S., Barretto, R., Habib, N., Hsu, P.D., Wu, X., Jiang, W., Marraffini, L.A., et al. (2013). Multiplex Genome Engineering Using CRISPR/Cas Systems. Science *339*, 819–823.

Crawford, E.D., Quan, J., Horst, J.A., Ebert, D., Wu, W., and DeRisi, J.L. (2017). Plasmid-free CRISPR/Cas9 genome editing in Plasmodium falciparum confirms mutations conferring resistance to the dihydroisoquinolone clinical candidate SJ733. PLOS ONE *12*, e0178163.

Dacheux, D., Landrein, N., Thonnus, M., Gilbert, G., Sahin, A., Wodrich, H., Robinson, D.R., and Bonhivers, M. (2012). A MAP6-Related Protein Is Present in Protozoa and Is Involved in Flagellum Motility. PLOS ONE *7*, e31344.

Delphin, C., Bouvier, D., Seggio, M., Couriol, E., Saoudi, Y., Denarier, E., Bosc, C., Valiron, O., Bisbal, M., Arnal, I., et al. (2012). MAP6-F Is a Temperature Sensor That Directly Binds to and Protects Microtubules from Cold-induced Depolymerization. J Biol Chem *287*, 35127–35138.

Edgar, R.C. (2004). MUSCLE: multiple sequence alignment with high accuracy and high throughput. Nucleic Acids Res *32*, 1792–1797.

Fang, F.C. (2004). Antimicrobial reactive oxygen and nitrogen species: concepts and controversies. Nat Rev Micro *2*, 820–832.

Gajria, B., Bahl, A., Brestelli, J., Dommer, J., Fischer, S., Gao, X., Heiges, M., Iodice, J., Kissinger, J.C., Mackey, A.J., et al. (2008). ToxoDB: an integrated Toxoplasma gondii database resource. Nucleic Acids Res *36*, D553–D556.

Gosling, R., and Seidlein, L. von (2016). The Future of the RTS,S/AS01 Malaria Vaccine: An Alternative Development Plan. PLOS Medicine *13*, e1001994.

Hall, N., Karras, M., Raine, J.D., Carlton, J.M., Kooij, T.W.A., Berriman, M., Florens, L., Janssen, C.S., Pain, A., Christophides, G.K., et al. (2005). A Comprehensive Survey of the Plasmodium Life Cycle by Genomic, Transcriptomic, and Proteomic Analyses. Science *307*, 82–86.

Han, Y.S., Thompson, J., Kafatos, F.C., and Barillas-Mury, C. (2000). Molecular interactions between Anopheles stephensi midgut cells and Plasmodium berghei: the time bomb theory of ookinete invasion of mosquitoes. The EMBO Journal *19*, 6030–6040.

Hwang, W.Y., Fu, Y., Reyon, D., Maeder, M.L., Tsai, S.Q., Sander, J.D., Peterson, R.T., Yeh, J.-R.J., and Joung, J.K. (2013). Efficient genome editing in zebrafish using a CRISPR-Cas

system. Nature Biotechnology *31*, 227–229.

Institute of Medicine (1991). Malaria: Obstacles and Opportunities (Washington, DC: The National Academies Press).

Janse, C.J., Carlton, J.M.R., Walliker, D., and Waters, A.P. (1994). Conserved location of genes on polymorphic chromosomes of four species of malaria parasites. Molecular and Biochemical Parasitology *68*, 285–296.

Janse, C.J., Ramesar, J., and Waters, A.P. (2006). High-efficiency transfection and drug selection of genetically transformed blood stages of the rodent malaria parasite Plasmodium berghei : Article : Nature Protocols. Nat. Protocols *1*, 346–356.

Janse, C.J., Kroeze, H., Wigcheren, A. van, Mededovic, S., Fonager, J., Franke-Fayard, B., Waters, A.P., and Khan, S.M. (2011). A genotype and phenotype database of genetically modified malaria-parasites. Trends in Parasitology *27*, 31–39.

Kanzok, S.M., Schirmer, R.H., Türbachova, I., Iozef, R., and Becker, K. (2000). The Thioredoxin System of the Malaria Parasite Plasmodium falciparum GLUTATHIONE REDUCTION REVISITED. J. Biol. Chem. *275*, 40180–40186.

Kearse, M., Moir, R., Wilson, A., Stones-Havas, S., Cheung, M., Sturrock, S., Buxton, S., Cooper, A., Markowitz, S., Duran, C., et al. (2012). Geneious Basic: An integrated and extendable desktop software platform for the organization and analysis of sequence data. Bioinformatics *28*, 1647–1649.

Kim, K., and Weiss, L.M. (2004). Toxoplasma gondii: the model apicomplexan. Int J Parasitol *34*, 423–432.

Kirkman, L.A., Lawrence, E.A., and Deitsch, K.W. (2014). Malaria parasites utilize both homologous recombination and alternative end joining pathways to maintain genome integrity. Nucleic Acids Res *42*, 370–379.

de Koning-Ward, T.F., Dixon, M.W.A., Tilley, L., and Gilson, P.R. (2016). Plasmodium species: master renovators of their host cells. Nat Rev Micro *14*, 494–507.

Lindner, S.E., Swearingen, K.E., Harupa, A., Vaughan, A.M., Sinnis, P., Moritz, R.L., and Kappe, S.H.I. (2013). Total and Putative Surface Proteomics of Malaria Parasite Salivary Gland Sporozoites. Mol Cell Proteomics *12*, 1127–1143.

Liu, J., Wetzel, L., Zhang, Y., Nagayasu, E., Ems-McClung, S., Florens, L., and Hu, K. (2013). Novel Thioredoxin-Like Proteins Are Components of a Protein Complex Coating the Cortical Microtubules of Toxoplasma gondii. Eukaryot Cell *12*, 1588–1599.

Mali, P., Yang, L., Esvelt, K.M., Aach, J., Guell, M., DiCarlo, J.E., Norville, J.E., and Church, G.M. (2013). RNA-Guided Human Genome Engineering via Cas9. Science *339*, 823–826.

Miller, L.H., Baruch, D.I., Marsh, K., and Doumbo, O.K. (2002). The pathogenic basis of malaria. Nature *415*, 673–679.

Montoya, J., and Liesenfeld, O. (2004). Toxoplasmosis. The Lancet *363*, 1965–1976.

Mulder, N.J., Apweiler, R., Attwood, T.K., Bairoch, A., Bateman, A., Binns, D., Bradley, P., Bork, P., Bucher, P., Cerutti, L., et al. (2005). InterPro, progress and status in 2005. Nucleic Acids Res *33*, D201–D205.

Müller, S. (2004). Redox and antioxidant systems of the malaria parasite Plasmodium falciparum. Molecular Microbiology *53*, 1291–1305.

Nakao, L.S., Everley, R.A., Marino, S.M., Lo, S.M., de Souza, L.E., Gygi, S.P., and Gladyshev, V.N. (2015). Mechanism-based proteomic screening identifies targets of thioredoxin-like proteins. J. Biol. Chem. *290*, 5685–5695.

Otto, T.D., Böhme, U., Jackson, A.P., Hunt, M., Franke-Fayard, B., Hoeijmakers, W.A.M., Religa, A.A., Robertson, L., Mandy Sanders, Ogun, S.A., et al. (2014). A comprehensive evaluation of rodent malaria parasite genomes and gene expression. BMC Biology *12*, 86.

Richie, T.L., Billingsley, P.F., Sim, B.K.L., James, E.R., Chakravarty, S., Epstein, J.E., Lyke, K.E., Mordmüller, B., Alonso, P., Duffy, P.E., et al. (2015). Progress with Plasmodium falciparum sporozoite (PfSPZ)-based malaria vaccines. Vaccine *33*, 7452–7461.

Sander, J.D., and Joung, J.K. (2014). CRISPR-Cas systems for editing, regulating and targeting genomes. Nat Biotech *32*, 347–355.

Shan, Q., Wang, Y., Li, J., Zhang, Y., Chen, K., Liang, Z., Zhang, K., Liu, J., Xi, J.J., Qiu, J.-L., et al. (2013). Targeted genome modification of crop plants using a CRISPR-Cas system. Nat Biotech *31*, 686–688.

Smith, R.C., Vega-Rodríguez, J., and Jacobs-Lorena, M. (2014). The Plasmodium bottleneck: malaria parasite losses in the mosquito vector. Mem Inst Oswaldo Cruz *109*, 644–661.

Straimer, J., Lee, M.C.S., Lee, A.H., Zeitler, B., Williams, A.E., Pearl, J.R., Zhang, L., Rebar, E.J., Gregory, P.D., Llinás, M., et al. (2012). Site-specific genome editing in Plasmodium falciparum using engineered zinc-finger nucleases. Nat Meth *9*, 993–998.

Tran, J.Q., Li, C., Chyan, A., Chung, L., and Morrissette, N.S. (2012). SPM1 Stabilizes Subpellicular Microtubules in Toxoplasma gondii. Eukaryotic Cell *11*, 206–216.

Turturice, B.A., Lamm, M.A., Tasch, J.J., Zalewski, A., Kooistra, R., Schroeter, E.H., Sharma, S., Kawazu, S.-I., and Kanzok, S.M. (2013). Expression of Cytosolic Peroxiredoxins in Plasmodium berghei Ookinetes Is Regulated by Environmental Factors in the Mosquito Bloodmeal. PLOS Pathogens *9*, e1003136.

Vonlaufen, N., Kanzok, S.M., Wek, R.C., and Sullivan Jr, W.J. (2008). Stress response pathways in protozoan parasites. Cellular Microbiology *10*, 2387–2399.

Wagner, J.C., Platt, R.J., Goldfless, S.J., Zhang, F., and Niles, J.C. (2014). Efficient CRISPR-Cas9-mediated genome editing in Plasmodium falciparum. Nat Meth *11*, 915–918.

Wakabayashi, K., and King, S.M. (2006). Modulation of *Chlamydomonas reinhardtii* flagellar motility by redox poise. J Cell Biol *173*, 743–754.

Whitelaw, J.A., Latorre-Barragan, F., Gras, S., Pall, G.S., Leung, J.M., Heaslip, A., Egarter, S., Andenmatten, N., Nelson, S.R., Warshaw, D.M., et al. (2017). Surface attachment, promoted by the actomyosin system of Toxoplasma gondii is important for efficient gliding motility and invasion. BMC Biology *15*, 1.

Wu, Y., Kirkman, L.A., and Wellems, T.E. (1996). Transformation of Plasmodium falciparum malaria parasites by homologous integration of plasmids that confer resistance to pyrimethamine. PNAS *93*, 1130–1134.

Xinzhuan Su, Hayton, K., and Wellems, T.E. (2007). Genetic linkage and association analyses for trait mapping in Plasmodium falciparum. Nature Reviews Genetics *8*, 497–506.

Zhang, C., Xiao, B., Jiang, Y., Zhao, Y., Li, Z., Gao, H., Ling, Y., Wei, J., Li, S., Lu, M., et al. (2014). Efficient Editing of Malaria Parasite Genome Using the CRISPR/Cas9 System. mBio *5*, e01414-14.

VITA

Kaitlyn Kiernan was born August 10, 1992 in Woodstock, IL. In May of 2015, she graduated from Loyola University Chicago with a Bachelor of Science in Biology with a Molecular Emphasis. In August of 2015, she began the Master of Science in Biology program at Loyola University Chicago. Here she was awarded a Graduate Fellowship and Tuition Scholarship for 2015-2017. After her master's, she will continue working in the microbiology field in Dr. Judith Behnsen's lab at the University of Illinois at Chicago. She also plans to pursue PhD programs in the Fall of 2018.